Acta Pharmaceutica Sinica B 2025;15(8):4225−4247

Chinese Pharmaceutical Association
Institute of Materia Medica, Chinese Academy of Medical Sciences

Acta Pharmaceutica Sinica B

www.elsevier.com/locate/apsb
www.sciencedirect.com

ORIGINAL ARTICLE

Improved prebiotic-based "shield" equipped probiotics for enhanced colon cancer therapy by polarizing M1 macrophages and regulating intestinal microbiota

Yang Wang[a,b,†], Xiaomin Su[a,b,†], Yao Liu[c], Lina Hu[b], Lin Kang[b], Ce Xu[a,b], Zanya Sun[a,b], Chenyu Sun[a,b], Huishu Guo[a,*], Shun Shen[b,*]

[a]*Central Laboratory, First Affiliated Hospital, Institute (College) of Integrative Medicine, Dalian Medical University, Dalian 116011, China*
[b]*Pharmacy Department, Shanghai Pudong Hospital, Fudan University Pudong Medical Center, Shanghai 201399, China*
[c]*Clinical Oncology Center, Shanghai Municipal Hospital of TCM, Shanghai University of Traditional Chinese Medicine, Shanghai 200071, China*

Received 15 February 2025; received in revised form 20 April 2025; accepted 27 April 2025

KEY WORDS

Lactobacillus reuteri;
NLRP3;
M1 macrophage;
Short-chain fatty acids;
Colon cancer

Abstract Probiotics play a crucial role in colon cancer treatment by metabolizing prebiotics to generate short-chain fatty acids (SCFAs). Colon cancer patients are frequently propositioned to supplement with probiotics to enhance the conversion and utilization of prebiotics. Nevertheless, the delivery and colonization of probiotics is hindered by the harsh conditions of gastrointestinal tract (GIT). Here, we devised a straightforward yet potent modified prebiotic-based "shield" (Gelatin-Inulin, GI), employing dietary inulin and natural polymer gelatin crosslinked *via* hydrogen bonding for enveloping *Lactobacillus reuteri* (*Lr*) to formulate synbiotic hydrogel capsules (*Lr*@Gl). The GI "shield" serves as a dynamic barrier, augmenting the resistance of *Lr* to gastric acid and facilitating its bioactivity and adherence in the GIT, synergizing with *Lr* to elicit an anti-tumor effect. Simultaneously, *Lr*@GI demonstrates anti-tumor effects by depleting glutathione to release reactive oxygen species, accompanied by the activation of NLRP3 (NOD-like receptor family pyrin domain containing 3), and the induction M1 macrophage polarization. Furthermore, *Lr*@GI can not only promote the recovery of intestinal barrier but also regulate intestinal flora, promoting the production of SCFAs and further exerting anti-tumor effect. Crucially,

*Corresponding authors.
E-mail addresses: guohuishu1@126.com (Huishu Guo), nanocarries@gmail.com (Shun Shen).
†These authors made equal contributions to this work.
Peer review under the responsibility of Chinese Pharmaceutical Association and Institute of Materia Medica, Chinese Academy of Medical Sciences.

https://doi.org/10.1016/j.apsb.2025.05.040

Lr@GI also potentiates the anti-tumor effect of 5-Fluorouracil. The construction and synergistic anti-tumor mechanism of synbiotic hydrogel capsules system provide valuable insights for gut microbial tumor therapy.

1. Introduction

Colon cancer is the predominant malignant neoplasm affecting the gastrointestinal tract (GIT)[1]. An increasing body of evidence suggests that the intestinal microbiota plays a pivotal role in the pathogenesis of inflammatory bowel disease, obesity, and carcinogenesis[2-4]. Probiotic therapies have gained recognition for their ability to restore the equilibrium between the immune microenvironment and gut microflora[5]. Nevertheless, the oral administration of probiotics is confronted with challenges including limited bioavailability in the hostile GIT and suboptimal colonization efficiency[6-8]. To overcome these obstacles, researchers have devised diverse strategies to safeguard the viability and effectiveness of probiotics, encompassing polymer-based techniques, surface mineralization, and biofilm encapsulation[9-16]. Regrettably, these approaches are hindered by their intricate production processes. Alternatively, fecal microbiota transplantation (FMT) offers a direct method for modulating microflora to treat digestive disorders[17]. However, the widespread adoption of FMT remains impeded due to the potential risk of infectious complications[18]. Therefore, it is imperative to establish a straightforward approach to enhance the survival and effectiveness of orally-administered probiotics to further advance bacterial therapy.

Microorganisms are an important component of ecosystems. The role of bacteria in the occurrence, development, and treatment of tumors has attracted widespread attention[15]. Various attenuated strains of *Salmonella typhimurium* and *Listeria monocytogenes* have been designed and engineered as targeted therapies or drug delivery vehicles for tumors, demonstrating excellent safety and therapeutic efficacy in mouse models[19-22]. Although these attenuated immunogenic bacteria have distinct advantages in treating diseases, the preparation of attenuated bacterial vaccines requires complex processes to ensure loss of pathogenicity while retaining immunogenicity. These processes require to be strictly controlled[23,24]. Moreover, its rapid proliferative capacity and inevitable immunogenicity limits its clinical application. Probiotics are known to have beneficial effects on host immunity overall, and they are considered safe for consumption and potentially therapeutic for cancer. Probiotics have their unique advantages over attenuated strains[25]. Probiotics help maintain intestinal health and balance by modulating the gut microbiota. They increase the number of beneficial bacteria and inhibit the growth of harmful bacteria, thereby reducing digestive system issues such as diarrhea and constipation[26]. Studies have shown that a single-cell coating composed of tannic acids and ferric ions, referred to as 'nanoarmor', can protect probiotics from the effects of antibiotics[27]. Additionally, probiotics are known as immune modulators, capable of enhancing overall immune function by influencing the intestinal immune system[28]. Previous studies have indicated that *Lactobacilli* can effectively ameliorate colorectal cancer. It has been reported that the *Lactobacillus* L*1681* and its derivative indole-3-lactic acid (ILA) can improve intestinal inflammation, tumor growth, and dysbiosis of the intestinal microbiota[29]. Furthermore, probiotics are widely accessible and easy to use as daily dietary supplements or as part of specific functional foods, suitable for a wide range of people. Compared to attenuated bacterial vaccines, probiotics are generally considered safe and harmless, causing no serious side effects or allergic reactions. Their long-term safety has been widely recognized and accepted. Currently, several probiotics have been identified as having beneficial effects[29-31], encompassing *Saccharomyces boulardii*, various species of *Lactobacillus* and *Bifidobacterium*, *Propionibacterium*, *Streptococcus*, *Bacillus*, *Enterococcus*, as well as specific strains of *Escherichia coli*. *Lactobacillus reuteri* (*Lr*), a species within the *Lactobacillus* genus, is widely present in the intestinal tracts of vertebrates and mammals[32]. It plays a crucial role in modulating immune responses, maintaining the gut microbiota balance, promoting beneficial metabolites, and preserving intestinal barrier function and morphology[33-35]. Importantly, *Lr* is acknowledged by the U.S. Food and Drug Administration (FDA) for its high safety profile in colicky infants and healthy adults, as demonstrated in a new drug trial[36]. Metabolomic analysis identified reuterin, which is produced by *Lr*, a natural colonizer of the human gut, as the most inhibitory compound[37]. Furthermore, study suggested that *Lr*, when present in a healthy gut microbiome, possessed inhibitory effect on colon cancer by altering the redox balance[38]. Previously, we developed a probiotic microgel delivery system (*Lr*@$(SA\text{-}CS)_2$) to improve intestinal flora dysregulation and enhance anti-tumor therapeutic effects through layer-by-layer encapsulation technology of alginate (SA) and chitosan (CS)[39]. Additionally, Bender et al.[40] demonstrated that dietary tryptophan metabolites released by *Lactobacillus tumefaciens* enhance the efficacy of immune checkpoint inhibitors. These findings highlight the potential of *Lr* for anti-tumor applications. However, it is essential to note that successful colonization and propagation in the intestinal milieu remain pivotal factors for the therapeutic efficacy of *Lr* against colon cancer.

The composite materials approved by the FDA have wide applications in the medical field, particularly in drug delivery, the approval of these composite materials by FDA mainly focuses on their biocompatibility, drug release characteristics, and safety[41,42]. While some drug-loaded composites, such as polylactic acid and polyvinyl alcohol composites have been approved for drug delivery systems and biodegradable implants[43-46], polyurethane can also be used for cardiovascular and soft tissue repair[47]. Although these materials exhibit certain biocompatibility, their degradation properties are poor, and byproducts such as lactic acid generated during the degradation process can potentially alter the local acidic environment of local tissues, affecting long-term safety[48,49]. Proteins and polysaccharides are often favored by researchers when choosing biomaterials for microbial cultivation. Additionally, various forms such as liquids, pills, enteric coatings, polymer gels, and dry powders have been developed for the oral

administration of probiotics[50-52]. Although these formulations have succeeded in improving delivery efficiency, the use of gut microbiota as oral therapeutic agents is largely limited. Hydrogel drug delivery systems have shown great potential and application prospects in the field of drug delivery, especially in improving drug efficacy and patient experience[53,54]. Prebiotics are substances that can be utilized by host bacteria to enhance the ratio of beneficial bacteria[55], thereby improving anti-tumor immunity[56]. Inulin, a natural fructan prebiotic, is widely employed in dietary applications due to its favorable safety profile and water solubility[57]. Notably, the metabolism of inulin by microorganisms leads to the production of short-chain fatty acids (SCFAs) with anti-tumor properties. Additionally, the presence of abundant hydroxyl groups in inulin permits robust cross-linking and hydrogel formation, which could enhance bio-adhesion and colonic retention[58]. Studies have demonstrated the advantageous colonic retention of inulin when formulated as a gel, effectively regulating the intestinal flora and fostering the proliferation of commensal microorganisms[59]. The University of Michigan reported an inulin gel-based oral immunotherapy that effectively reshape the small intestinal microbiome and metabolites to establish specific oral tolerance to allergens and achieve effective suppression of food allergy in a mouse model of food allergy[60]. Nevertheless, inulin demonstrates a restricted capacity for gel formation, and an excessive intake may potentially contribute to indigestion and gastrointestinal dysfunction. In an endeavor to mitigate these challenges, the integration of natural polymer has been explored to facilitate gel formation and reduce the reliance on inulin. Collagen is highly suggested for hydrogel-mediated tissue engineering, because of its desirable effect on cell adhesion, migration, and proliferation[61]. Nevertheless, its high cost poses a significant drawback. Consequently, gelatin can be considered as a viable alternative owing to its non-immunogenic nature and cost-effectiveness, while retaining several unique properties, such as high biocompatibility, absence of skin irritation, and favorable cell attachment[62-64]. In addition, gelatin provides arginine-glycine-aspartic acid (RGD) peptide sequence that imparts favorable cell adhesion capacity to hydrogels made by this polymer[65]. Furthermore, the structural stability of gelatin in acidic environments and its alkaline decomposition properties make it more resistant to the harsh stomach acid environment[66]. To date, the available literature predominantly focuses on the use of inulin for drug delivery in the context of colitis treatment, primarily centered on its potential to modulate the intestinal flora of host and exert anti-inflammatory effect. The potential therapeutic effect of inulin as a prebiotic camouflaged probiotic in synbiotic gels for colon cancer is still uncertain.

Herein, we designed to construct a biocompatible gelatin-inulin (GI) hydrogel "shield" system based on the prebiotic inulin and the polymer gelatin by a simple hot-cold alternating method. The GI "shield" was employed to encapsulate *Lr* for the formulation of synbiotic hydrogel capsules (*Lr*@GI). As shown in Fig. 1, the GI "shield" not only serves as a dynamic barrier, enhancing the resistance of *Lr* to gastric acid stress, but also contributes to the intestinal colonization of *Lr*, synergistically exerting an anti-tumor effect with *Lr*. Furthermore, *Lr*@GI can promote the recovery of intestinal barrier and generate a significant amount of short-chain fatty acids (SCFAs) through the fermentation of the prebiotic inulin, which positively influences the intestinal flora and produces anti-tumor effect. Additionally, upon orally administered, synbiotic hydrogel capsules *Lr*@GI releases reactive oxygen species (ROS) by depleting glutathione (GSH), triggers the production of pro-inflammatory factors by activating NOD-like receptor family pyrin domain containing 3 (NLRP3), and inhibits tumor growth through the polarization of M1 macrophages. Crucially, this synbiotic hydrogel capsules *Lr*@GI also potentiates the anti-tumor effect of chemotherapeutic drug 5-Fluorouracil (5-FU). The favorable biocompatibility and uncomplicated manufacturing process of *Lr*@GI indicate its potential for clinical translation.

2. Materials and methods

2.1. Mateials

Inulin and gelatin were obtained from Aladdin Reagent Company (Aladdin, Shanghai, China). FITC-Inulin was obtained from Sigma−Aldrich (Shanghai, China). Pepsin, trypsin, bile salts, antibiotics were purchased from McLean Reagent Company (McLean, Shanghai, China). ELISA kits (TNF-α, IL-1β) were purchased from Lianke Biologics (Shanghai, China). Bcl-2, Bax and β-actin antibodies were purchased from CST website (USA). NLRP3, ZO-1, iNOS, Arginase antibodies were obtained from Proteintech (Wuhan, China). DCFH-DA-Reagent was obtained from Tongren Chemical (Japan). CD11b, CD45, CD206, CD86 flow antibodies were obtained from Biolegend Reagent Company. Cell counting kit-8 (CCK-8) was obtained from KeyGen BioTech (Nanjing, China). BCA protein concentration detection reagent and GSH detection reagent were provided by Biosharp (Shanghai, China). 1640 complete medium was purchased from Fuheng (Shanghai, China), trypsin-ethylene diamine tetraacetic acid (EDTA, 0.05%) and fetal bovine serum were purchased from Life Science (Gibco, Pittsburgh, USA). CT26 cell line was provided by the School of Pharmacy, Fudan University. *Lactobacillus reuteri* (*Lr*) and MRS medium were obtained by BiouBowei Biotechnology Co., Ltd. (Beijing, China). H&E kit, TUNEL apoptotic reagent and Ki67 antibody were supplied by Servicebio (Wuhan, China).

Male BALB/c mice with SPF grade of 5−6 weeks 20−25 g were provided by Shanghai Yisheng Biological Company (Shanghai, China). All mice were housed in a specific pathogen-free experimental at medical center of Shanghai Pudong Hospital, Fudan University. The animal experiment was approved by the Ethics Committee of Shanghai Pudong Hospital (2022-KY-01).

2.2. Preparation and characterization of Lr@GI

Firstly, we prepared hydrogel by adjusting the methods described in the literatures, 300 mg of inulin was weighed, and dissolved in 1 mL of distilled water, and 20 mg of gelatin was added to another 1 mL of distilled water, the mixture was heated in a water bath at 70 °C for 5 min. The gelatin solution was slowly dripped into the inulin solution to obtain the hydrogel GI. After standing at room temperature, *Lr* (10^8 CFU/mL) was added into the hydrogel GI, stirred to uniformity with a magnetic stirrer and left at room temperature overnight to obtain *Lr*@GI. The morphologies of *Lr* and *Lr*@GI were characterized by SEM (HITACHI Regulus 8100, Japan). The samples of each group were collected and fixed for dehydration, the samples were fixed with 2.5% glutaraldehyde, rinsed with phosphate buffer three times, then fixed with 1% osmic acid for 4−6 h, followed by gradient dehydration with ethanol, and then replaced with isoamyl acetate twice, 20 min/time. CO_2 critical point drying was carried out. Finally, after the ion

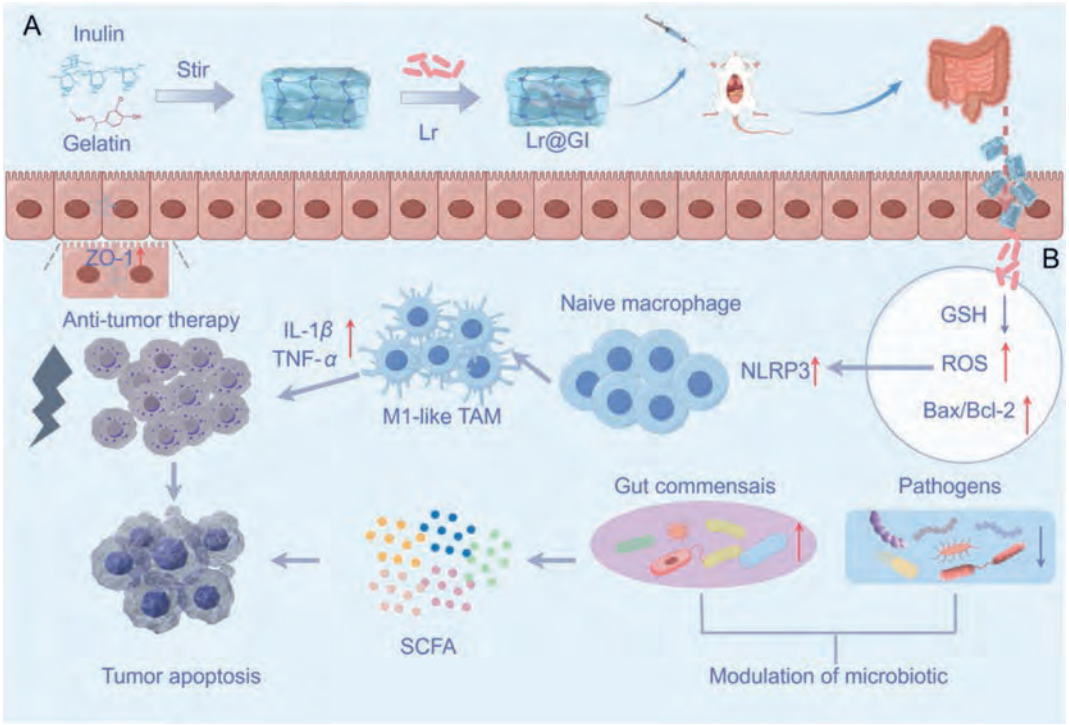

Figure 1 Schematic illustration of synbiotic hydrogel capsules for colon cancer treatment by polarizing macrophage polarization and regulating intestinal microbiota. (A) Preparation of *Lr*@GI. (B) The proposed therapeutic mechanisms of *Lr*@GI.

sputtering gold, it could be observed and photographed by scanning electron microscope. For CLSM, *Lr* was incubated with DAPI on dark room ice for 10 min and washed with PBS. Then, *Lr* was incubated with FITC-GI for 30 min and washed with PBS. FTIR (Thermo Fisher Scientific Nicolet iS20, USA) qualitatively analyzes the sample by obtaining infrared absorption spectra of transmittance or absorbance with wave length. In a dry environment, the ATR attachment is placed in the optical path of the spectrometer, when the air background is scanned, the sample is dropped on the crystal surface of the ATR attachment, and then the infrared spectrum of the sample is collected with a resolution of 4 cm^{-1}, the number of scans is 32, and the range of the test wavelengths is 400/600−4000 cm^{-1} (according to the test requirements), and the infrared absorption spectrograms of the transmittance versus the wavelength are obtained. The particle size and potential of inulin, gelatin, GI, *Lr*, and *Lr*@GI were detected by DLS. Additionally, the viscosity and rheological properties of *Lr*@GI were tested on a 20 mm sandblasted parallel plate using perjeta temperature control plate and cover plate (Anton Parr MCR702 rheometer, Austria). Using a pipette, take a small amount of *Lr*@GI and place it on the rheometer platform. When the flat plate rotor contacts the sample and is squeezed, the plate rotor is locked and wipe away the extruded sample, then click "Start" to conduct rheological determination of *Lr*@GI under specific conditions.

2.3. *Gastrointestinal resistance of GI "shield" and intestinal retention of Lr@GI*

The retention capacity of GI hydrogel in GIT was investigated *in vivo*: BALB/c mice were individually administered 100 μL of FITC-Inulin/FITC-GI hydrogel solution *via* gastric gavage and euthanized at different time points (2, 4, 6, 10, 12 h) ($n = 3$). Intestinal tissues were collected for IVIS imaging to observe the retention of both substances in the colon (and cecum). Secondly, the resistance of *Lr*@GI to simulate GIT was studied *in vitro*: 100 μL of *Lr* and *Lr*@GI with the same bacterial count were suspended in SGF (pH = 2), SIF (pH = 6.8), 3% bile salt solution, and 7.5 mg/mL antibiotic solution respectively, The samples were cultured in a constant temperature incubator at 37 °C, 100 μL samples were collected, centrifuged, washed and diluted with PBS at different time points, the appropriate amount of diluted bacterial solution is plated on the MRS solid agar plate. The number of colonies was counted after incubation for 24 h. Finally, the resistance of *Lr*@GI in the GIT was studied *in vivo*: The male BALB/c mice were individually administered 100 μL of *Lr* or *Lr*@GI solution *via* gastric gavage and sacrificed at specific time points. The contents of stomach, small intestine, cecum, and colon were collected, homogenized and diluted with PBS, plated 100 μL bacterial solutions onto MRS solid agar plate. The number of colonies was counted after incubation for 24 h.

2.4. *The biological safety study*

The safety of orally administered *Lr*@GI was assessed by blood routine and blood biochemistry. 50 μL of whole blood was extracted from each mouse orbit using a capillary glass tube. The blood intended for blood routine examination was preserved in purple vacutainer tubes containing EDTA anticoagulant, while the blood for biochemical analysis was preserved in EP tubes. Quantitative analysis was performed using a standard animal blood analyzer. 50 μL whole blood was extracted from each mouse orbit using a capillary glass tube. Blood for routine

testing is stored in a purple collection vessel containing EDTA anticoagulant, and blood for blood biochemistry is stored in an EP tube containing heparin lithium. Quantitative analysis was performed using a standard animal blood analyzer. To assess the safety of *Lr*@GI in intestinal tissues, a fluorescent probe called FITC-Dextran was utilized for precise evaluation of intestinal permeability. Healthy mice were administered different formulations the day before the experiment. After fasting for 4 h the next day, each mouse received 200 μL (25 mg/mL) of FITC-Dextran solution by gavage and continued fasting for 3 h.

2.5. The distribution of Lr@GI in tumor tissue

The distribution of *Lr* in the tumor: Based on the gene sequence of *Lr*, we designed the corresponding primers: forward 5′-TGGGCGCAAGCCTGATGGA-3′, reverse 5′-TGAACAGTTACTCTCACGCACG-3′. DNAiso Reagent was added to the tumor tissue and homogenizaed with homogenizer. The lysate was added to tissue and centrifuged at 1000×*g* for 10 min at 4 °C to obtain the supernatant, then half volume of anhydrous ethanol was added for vortex centrifugation to discard the supernatant. Subsequently, 1/2 volume of 75% ethanol was added for vortex centrifugation to discard the supernatant, and enzyme-free water was added to obtain DNA, which was directly used for PCR reactions followed by DNA gel electrophoresis. Furthermore, tumor tissue of each group was collected, homogenized and diluted with PBS, 100 μL bacterial solution was plated onto MRS solid agar plate, the number of colonies was counted after incubation for 24 h.

2.6. In vivo anti-tumor study

The anti-tumor properties of *Lr*@GI were evaluated in mice with in orthotopic colon cancer. Firstly, we established an orthotopic cancer model. The modeling method for *in situ* colon cancer involved the use of whole-cell cytoplasmic injection. Mice were anesthetized with isoflurane, and an incision was made in the left lower abdomen. The incision was disinfected, revealing that the cecum had been extracted from the left lower abdomen and pulled out through the incision. A total of 100 μL of 5×10^6 CT26 cells suspended in saline were injected subserosally into the vascular area of the mid-cecum using a 1 mL syringe. After the injection, the needle was removed, and a small cotton ball was pressed against the site for 30 s. After the injection liquid was absorbed by the intestinal wall, the abdominal cavity was washed with saline, the cecum was reset to avoid pressure, and the abdominal cavity was closed. The sham surgery group underwent the same surgical procedure except for the cell injection. The entire surgical process adhered to sterile surgical principles, and no antibiotics were used postoperatively. After modeling, all mice were placed in SPF animal cages for routine feeding for 8 days, and tumor growth was monitored by IVIS *in vivo*. On Day 8 after the establishment of the model, mice were randomly divided into 5 groups, the mice were treated once every two days and given five times of intragastric administration. the tumor volume and body weight of mice were recorded every other day for 20 days. After 20 days, the tumor tissue was stained with H&E, Ki67, and TUNEL to evaluate its anti-tumor effect, the major organs were stained with H&E to evaluate biological safety.

2.7. CCK-8 toxicity detection

The cytotoxicity of different concentrations of GI (0, 200, 400, 800, 1600, 2000 μg/mL) and different bacterial amounts of *Lr* (10^3, 10^4, 10^5, 10^6, 10^7, 10^8 CFU/mL) to CT26 was detected. To investigate the anti-tumor effect of *Lr*@GI *in vitro*, CCK-8 assay kit is used to detect the cytotoxicity of *Lr*@GI. Initially, CT26 cells were inoculated on 96-well plates with 10^4 cells per well and incubated for 24 h, then treated with different drugs for 24 h, culture medium was removed, and 100 μL of diluted CCK-8 was added to the pore plate. The 96-well plates were placed in incubator at 37 °C and incubated for 1−2 h away from light. The OD value was detected by microplate reader at 450 nm absorbance wave length. Cell viability was calculated based on these measurements.

2.8. Detection of GSH

Initially, CT26 cells were inoculated on 96-well plates with 10^4 cells per well and incubated for 24 h. After each group was treated with different drugs for 24 h, the cells were washed with pre-cooled PBS, and collected by cell scraper. Cells were lysed with Triton-X-100 and lysed for 20 min on ice, then centrifuged at 1000×*g* for 10 min at 4 °C and supernatant was obtained. Appropriate amount of supernatant was mixed with 200 μL DTNB and incubated for 30 min. OD values of cells in each group were detected by microplate reader (Thermo Fisher Varioskan LUX, USA) at A_{412} nm absorbance wave length. The same method was used to assess GSH levels *in vivo*.

2.9. Detection of ROS

Following the above steps, CT26 cells were treated with different drugs, washed with PBS twice, and finally added 100 μL diluted DCFH-DA (10 μmol/L) and incubated for 30 min in dark light to detect ROS expression in CT26 cells. DAPI-labeled nuclei were incubated for 10 min. The fluorescence of DCFH was observed by laser scanning confocal microscope (CLSM, Carl Zeiss, LSM710, Oberkohen, Germany) or flow cytometry (Agilent, NovoCyte 3000. USA). DHE was used to reflect ROS levels *in vivo*.

2.10. Detection of TNF-α and IL-1β cytokines

Cytokines TNF-α and IL-1β were detected by ELISA. CT26 cells were inoculated on 6-well plates with 10^5 cells per well and incubated for 24 h, then treated with different reagents for 24 h. Subsequently, each group was centrifuged at 1000×*g* for 5 min, washed twice with PBS and centrifuged at 300×*g* for 10 min to collect the supernatant. According to the protocols by ELISA kit. The methods of serum cytokine detection were the same.

2.11. Western blot

Briefly, CT26 cells were inoculated on 6-well plates with 10^5 cells per well and incubated for 24 h, followed by treatment with different drugs for 24 h. After washing twice with pre-cooling PBS, appropriate amount of lysis was added to each well for 20 min, which was centrifuged 12,000×*g* at 4 °C for 10 min. The protein concentration of each group was measured by BCA

protein concentration kit. OD values of each group were detected by microplate reader at 562 nm absorbance wave length, and protein concentrations were calculated according to OD values. After quantification with protein loading buffer and PBS, the diluted protein solutions were heated at 95 °C for 10 min, and immediately placed in the −20 °C refrigerator. Next, after electrophoresis, SDS-PAGE gel was transferred onto PVDF membrane, after incubate with a blocking solution for 1 h, then PVDF membrane was incubated with related antibodies at 4 °C overnight. The next day, after washing the PVDF membrane with TBST for three times, the PVDF membrane incubated with HRP-labeled goat anti-rabbit antibody for 1 h, followed by another three washes with TBST. Imaging was conducted by Bio-RAD (ChemiDoc Go, USA). The detection of tissue protein was consistent with the above.

2.12. Detection of macrophage polarization

To prove the immune response of tumor cells induced by *Lr*@GI. CT26 cells were treated with different reagent, and then the treated CT26 cells were co-cultured with RAW264.7 cells. The collected cells were incubated with F4/80, CD86 and CD206 flow antibodies for 30 min respectively, after PBS washing, the polarization of macrophages was detected by flow cytometry. To evaluate the immune response triggered by *Lr*@GI *in vivo*, the tumors were collected at 10 days after treatment and cut into small pieces, then the tissue was digested with collagenase V (2 mg/mL, YEASEN) in HBSS solution for 4 h at 37 °C. Single-cell suspensions were obtained by filtering cells through a 70-μm cell strainer and washed with FACS buffer. The prepared single-cell suspensions were stained with fluorescent antibodies against CD11b, CD45, F4/80, CD86, and CD206 for 30 min. After washing with FACS buffer, flow cytometry was used to assess the polarization of macrophages. The data was analyzed using FlowJo.

2.13. Fecal SCFA detection and SCFA in medium supernatant by GC−MS

On Day 18 after in orthotopic colon cancer treatment, fresh faecal pellets were collected from mice and appropriate amount of faeces was homogenised in deionised water and centrifuged at 3000×*g* for 5 min at 4 °C. The supernatant was taken and the pH of the supernatant was measured by pH meter. For the measurement of SCFAs, we used Milli-Q water to extract SCFA from faecal pellets. An appropriate amount of pure standard solutions of 7 SCFAs (acetic acid, propionic acid, butyric acid, isobutyric acid, valeric acid, and isovaleric acid) were taken to prepare 100 mg/mL stock solution by mixing with water, which was further diluted with water to obtain a series of working standard solutions. A proper amount of pure standard acetic acid was taken and mixed with ether to prepare 100 mg/mL stock solution, which was further diluted with ether to obtain a series of the reserve solutions. The internal standard (4-methylpentanoic acid) was prepared into 375 μg/mL with ether, Ten standard curve points were prepared by mixing 200 μL working standard solution of series of 6 acids, 100 μL 15% phosphoric acid, 20 μL working standard solution of series of hexanoic acid, 20 μL internal standard and 260 μL ethyl ether at the following concentrations: 0.02, 0.1, 0.5, 2, 10, 25, 50, 100, 250, and 500 μg/mL 100 μL of 15% phosphoric acid, 20 μL of hexanoic acid working standard solution, 20 μL of the internal standard, and 260 μL of ether. The stock solutions were stored at −20 °C, and the working solutions were prepared freshly. Appropriate sample was taken into a 1.5 mL centrifuge tube, add 500 μL water and add 100 mg glass beads in 1.5 mL centrifuge tube, homogenized for 1 min and centrifuged at 12,000 rpm at 4 °C for 10 min, and 200 μL of the supernatant was collected and 100 μL of 15% phosphoric acid and 20 μL of 375 μg/mL internal standard (4-methylvaleric acid) solution were added, followed by mixing with 280 μL of ether for 1 min, the mixture was then centrifuged at 12,000 rpm at 4 °C for 10 min, and the supernatant was tested on the machine. The experimental analysis was performed on trace 1300 gas chromatograph (Thermo Fisher Scientific, USA). Mass spectrometric detection of metabolites was performed on ISQ 7000 (Thermo Fisher Scientific, USA). SCFAs in medium supernatants are detected in the same way.

2.14. 16S rDNA sequencing

The CT26 orthotopic tumor mice were administered according to the above method. On Day18, fecal pellets were obtained and preserved at −80 °C for subsequent microbiological analysis. Microbial DNA was extracted and the DNA was quantitatively analyzed by Nanodrop, and the quality of DNA extraction was detected by 1.2% agarose gel electrophoresis. Typically, the target sequences that can reflect the composition and diversity of bacterial flora. the target sequences reflective of microbial community composition and diversity of bacterial flora, such as microbial ribosomal RNA or specific gene fragments are usually taken as targets. The corresponding primers were designed according to the conserved regions in the sequences. The specific barcode sequence of the sample was added, and then PCR amplification was performed on the variable region of rRNA gene (single or multiple consecutive regions) or specific gene fragments. Fluorescence quantification was performed on the PCR amplification products by Quant-iT PicoGreen dsDNA Assay Kit and measured by Microplate reader (BioTek, FLx800, USA). Based on the fluorescence quantitative results, the samples were proportionally mixed according to the sequencing quantity required for each sample. Illumina's TruSeq Nano DNA LT Library Prep Kit was used to prepare sequencing libraries. High-throughput sequencing was conducted on the computer. The library and samples were divided according to index and Barcode information from the original sequence of quality preliminary screening, and barcode sequence was removed. Subsequently, following the analysis flow of QIIME2 dada2 or Vsearch software for sequence denoising or OTU clustering, the specific composition of each sample (group) at different species taxonomic levels was displayed to understand overall microbial profile.

2.15. Histopathological examination

To make a thorough inquiry the biocompatibility of the *Lr*@GI *in vivo*, the body weight of BABL/c mice was recorded every other day during treatment. On Day 20, the mice were euthanized, and major organs (heart, liver, spleen, lung, kidney) were dissected for H&E staining. Additionally, tumor tissues were subjected to TUNEL and Ki67 staining to assess relevant pathological changes related to the anti-tumor efficacy *in vivo*.

2.16. Statistical analysis

All analyzed data are presented as mean ± standard deviation. The student's *t*-test was used to compare differences between the two

groups, where "ns" indicates no significant difference. Multiple group analyses were performed using GraphPad 8 *via* one-way analysis of variance (ANOVA). $*P < 0.05$, $**P < 0.01$, $***P < 0.001$, represent statistical differences.

3. Results

3.1. Preparation and characterization of synbiotic hydrogel capsules Lr@GI

Dietary inulin was employed as the prebiotic instrumental in the development of the hydrogel. The rationale for choosing inulin stems from its recognition by the FDA as a dietary fiber that enhances the antitumor efficacy of anti-programmed cell death protein-1 (α-PD-1) therapy[58,67]. Furthermore, the metabolic byproducts produced by probiotics fermenting inulin in the colon trigger the multiplication of advantageous *Bifidobacteria* and *Lactobacilli* in the intestinal microbiota. This process contributes to the enrichment and diversity of the intestinal microbial community[68,69]. To facilitate the formation of the hydrogel, we introduced the natural polymer gelatin, renowned for its superior biocompatibility and degradability[70]. The GI hydrogel was formed by inulin and gelatin as raw materials *via* a simple heating-cooling method. In previous experiments, it was observed that the formation of hydrogel using inulin alone posed challenges, the introduction of gelatin proved to be conducive to the successful formation of the hydrogel. This was attributed to the strong cross-linking between the abundant hydroxyl groups in inulin and the carboxyl and amino groups in gelatin, promoting hydrogel formation (Fig. 2A). The scanning electron microscopy (SEM) images shown that *Lr* has a smooth surface with no additional material attached, reflecting the natural morphology of the bacteria. In contrast, *Lr*@GI exhibited a rough and grainy surface. This roughness might be attributed to the irregular covering layer formed by the GI hydrogel on the bacterial surface (Fig. 2B). To further verify the encapsulation success and the presence of *Lr*@GI as individual granules, the GI labeled with green fluorescence was fused with *Lr*, which was labeled with blue fluorescence. As illustrated in Fig. 2C, following the immobilization of *Lr*@GI in glycerol, distinct co-localization of green and blue fluorescence was observed using laser scanning confocal microscopy (CLSM). The bacteria appeared more loosely aligned without significant aggregation. These results suggested that *Lr* can be effectively encapsulated by the GI hydrogel, allowing *Lr*@GI to exist in a more dispersed form rather than in large aggregates. Subsequently, the interaction between inulin, gelatin, and GI hydrogel was evaluated by Fourier transform infrared spectroscopy (FTIR). A noteworthy phenomenon in the infrared spectra of inulin was the emergence of a broad band at 3422.92 cm^{-1}, representing the −OH stretching vibration and hydrogen bonds in the polysaccharid[71]. Gelatin exhibited a broader band at 3280.80 cm^{-1} due to −NH tensile vibrations of amide groups and free −OH groups in its structure. In the spectrum of GI, the broad band of −OH stretching vibration was centered at 3412.01 cm^{-1}. The −OH band slightly shift towards lower wavenumbers after the formation of GI. In addition, the C═O stretching vibration band of inulin at 1646.95 cm^{-1} merged with the absorption band of gelatin at 1626.27 cm^{-1} to form a broad bond at 1639.82 cm^{-1} in the GI hydrogel spectrum. The reason was that the vibration frequencies of the related functional groups (such as hydroxyl or carbonyl) decrease when hydrogen bond was formed, which enhanced the intermolecular interactions and reduced the energy required for vibration[72,73]. It contributed to a redshift of the absorption peak. In many cases, the variation of the −OH stretching vibration can more clearly reflect the formation of hydrogen bonds[74], which we found in the previous study as evidence of hydrogen bond formation. Moreover, the N−H vibration of inulin at 1551.64 cm^{-1} in the amide II region merged with the absorption band of gelatin at 1528.49 cm^{-1}, while the N−H vibration in the amide II of GI was weaker, which may be due to the influence of hydrogen bonding on its vibration. Furthermore, the C−O stretching vibration band of gelatin at 1078.84 cm^{-1} merged with the absorption band of inulin at 1030.11 cm^{-1}, and a broad bond at 1031.48 cm^{-1} is also observed in the FTIR spectrum of GI[75] (Fig. 2D). The foregoing result indicated that the hydroxyl groups of inulin and the carboxyl and amino groups of gelatin cross-link with each other to form hydrogels. To investigate the property of GI hydrogel, a rheometer was employed to analyze the rheology and viscosity of hydrogel. In rheological analysis experiments, sample was classified a solid rather than a liquid when the storage modulus (G′) exceeds the loss modulus (G″)[76]. As depicted in Fig. 2E, G′ was notably greater than G″, providing evidence for the formation of hydrogel by GI. Furthermore, the relationship between hydrogel viscosity and shear rate was examined, as illustrated in Fig. 2F. The viscosity of GI hydrogel exceeded that of inulin and gelatin, following further analysis revealed the viscosity of GI hydrogel progressively decreased with increasing shear rate, indicating the presence of shear-thinning behavior within the hydrogel. The result showed that the structure of the GI hydrogel had a certain degree of flexibility and variability.

The particle size and zeta potential of each group were characterized, it was observed that the particle size of *Lr*@GI increased by 200 nm compared to *Lr* (Fig. 2H), which was attributed to the successful wrapping of *Lr* by GI. Additionally, the potential of GI-armed *Lr* changed from −35 to −28 mV (Fig. 2G), probably due to the surfaces of bacteria usually carry a negative charge[77], and the GI gel may adsorb ions in solution, which could alter the distribution or flow of surrounding charges, potentially resulting in an increase in electric potential and thus affecting its zeta potential. In general, the increased potential after GI gel coating *Lr* may be due to uneven charge distribution on the surface of the GI gel or its inherent electric field shielding effect. These factors changed the electric field distribution around the material, affecting the measured potential values[78]. These findings affirmed the successful synthesis of the synthetic hydrogel capsules *Lr*@GI. Subsequently, to validate whether GI encapsulation affected the viability of *Lr*@GI, the growth curve and vitality of both *Lr* and *Lr*@GI were monitored, respectively. As shown in Fig. 2I, the growth rate of *Lr* was faster than that of *Lr*@GI in the first 8 h potentially related to the encapsulation of GI. However, the two groups eventually reached the same optical density (OD 600) at 22 h, which proved that the use of GI as shield to protect *Lr* did not affect its growth. Furthermore, AlamarBlue, a redox indicator that undergoes absorbance and fluorescence changes based on metabolic activity, was used to monitor bacterial viability. The results, as illustrated in Fig. 2J, revealed no significant decrease in bacterial viability of *Lr*@GI over time compared to *Lr*, demonstrating that GI acting as a shield to camouflage *Lr* did not compromise bacterial survival.

3.2. *Study of gastrointestinal resistance of GI "shield" and intestinal retention of synbiotic hydrogel capsules Lr@GI*

To verify whether the adhesive capacity of GI "shield" increases intestinal retention, FITC-labeled inulin and GI were employed for oral administration and imaged using *in vivo* imaging system (IVIS) at different time points to observe the retention of them in the intestinal tract[67]. Results depicted in Fig. 3A and Supporting Information Fig. S1 revealed notably higher fluorescence intensity of GI compared to inulin after 6 h, indicating that the cross-linked inulin and gelatin enhanced the gastrointestinal retention of GI. The harsh environment of the GIT is not conducive to the survival of *Lr*. After oral administration, the strong acidic gastric juice, various digestive enzymes and bile salts in the intestine could lead to mortality of probiotic, which further cause the limited colonization and proliferation ability of probiotics in the GIT[79]. Consequently, the survival rate of *Lr*@GI in the harsh GIT was explored. To elaborate, equal amounts of *Lr* and *Lr*@GI were incubated in simulated gastric fluid (SGF) at pH = 2, 3% bile salts (BS), simulated intestinal fluid (SIF) at pH = 6.8 and 7.5 mg/mL antibiotic solution respectively. Subsequently, they were plated on MRS agar plates at different time points to calculate the number of colonies (Supporting Information Fig. S2A−S2D). The results indicated that the survival rate of *Lr*@GI in SGF was 1.6 times higher than that of *Lr* at 2 h. Although both survival rates decreased at 4 h, *Lr*@GI still exhibited twice the survival rate of *Lr*. As expected, the GI "shield" could enhance survival rate of *Lr* in gastric acid, which was in stark contrast with extensive deactivation of *Lr* (Fig. 3B). Comparable protection effect was observed for *Lr*@GI that was incubated with BS, SIF, and antibiotic solution respectively, indicating that GI acts as a protective "shield" against adverse

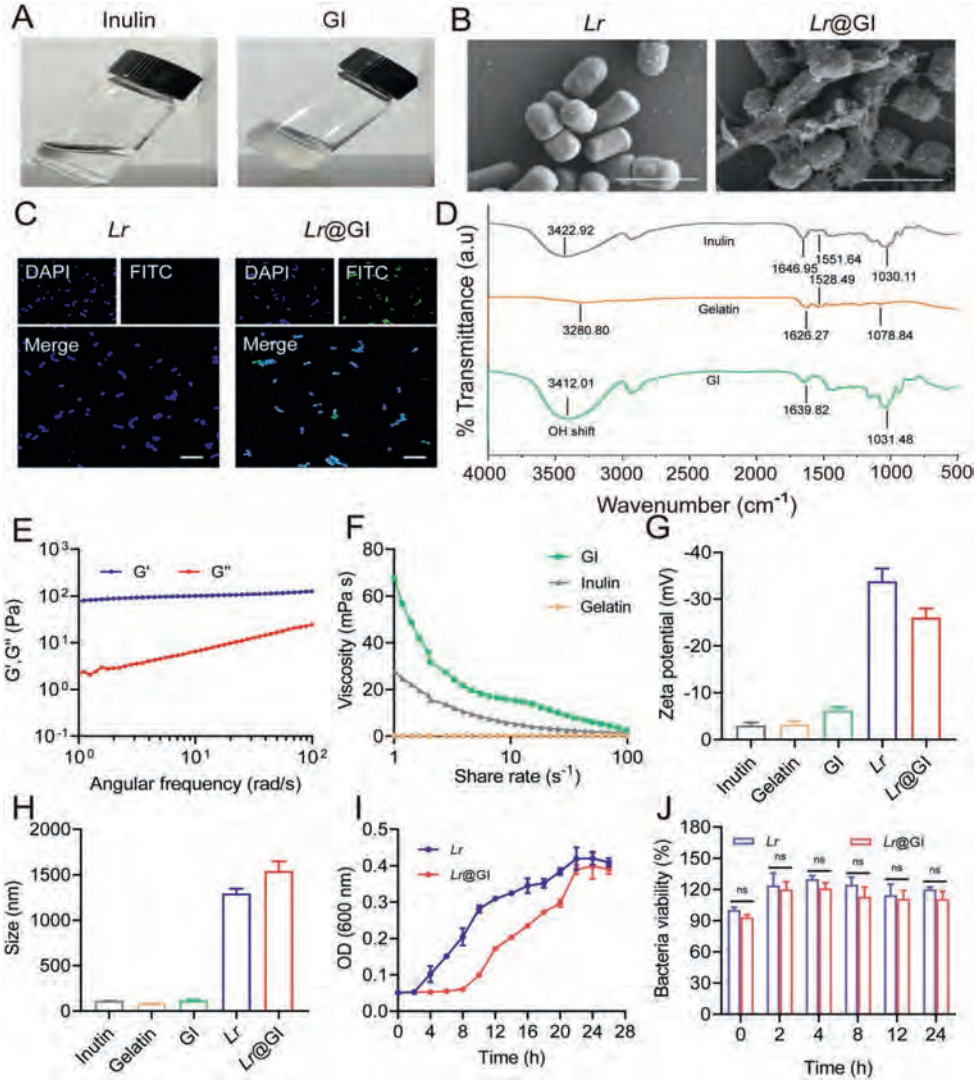

Figure 2 Preparation and characterization of *Lr*@GI. (A) The visual appearance and structure of inulin and hydrogel GI. (B) The SEM images of *Lr* and *Lr*@GI (scale bar = 2 μm). (C) LSCM images of *Lr* and *Lr*@GI. The bule channel shows *Lr*, the green channel shows FITC-GI, and the merge shows *Lr*@GI. (scale bar = 10 μm). (D) The FTIR spectra of inulin, gelatin, GI hydrogel. (E) The rheological properties detection of *Lr*@GI. (F) The viscosity test of inulin, gelatin, and hydrogel GI. (G) Dynamic Light Scattering size distribution and (H) zeta potential inulin, gelatin, GI, *Lr*, and *Lr*@GI. (I) The growth curves of *Lr* and *Lr*@GI. (J) Bacterial viability of *Lr* and *Lr*@GI at different time points by AlamarBlue staining assays. Data are presented as mean ± SD (n = 5). ns, not significant.

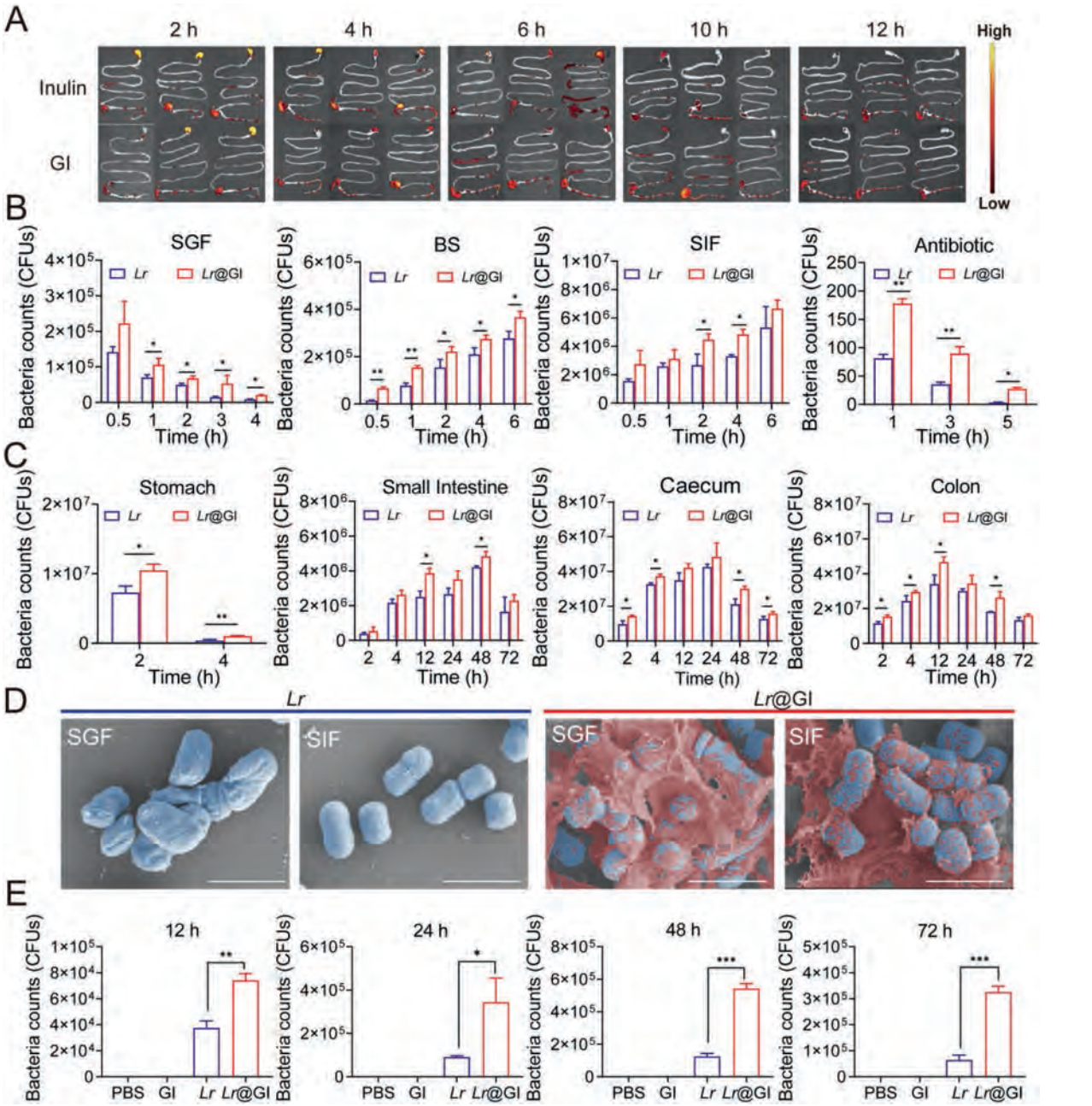

Figure 3 The intestinal retention of GI and gastrointestinal resistance of *Lr*@GI. (A) Retention of inulin and GI hydrogels at different time points *in vivo* ($n = 3$). (B) The bacterial quantitative analysis of *Lr* and *Lr*@GI in SGF, BS, SIF, and antibiotic at different time ($n = 3$). (C) The bacterial quantitative analysis in stomach, small intestine, cecum and colon after administration of *Lr* and *Lr*@GI at different time points ($n = 3$). (D) The SEM images of *Lr* and *Lr*@GI after incubation in SGF and SIF for 2 h (scale bar = 2 μm). (E) The bacterial quantitative analysis in tumor after oral administration of PBS, GI, *Lr* and *Lr*@GI. Data are presented as mean ± SD ($n = 3$). $^{*}P < 0.05$, $^{**}P < 0.01$, $^{***}P < 0.001$. ns, not significant.

environments. Subsequently, to quantify the survival of *Lr* and *Lr*@GI in the GIT, the amount of living *Lr* inside the stomach, small intestine, cecum, and colon was detected by plate counting (Supporting Information Fig. S3A−S3D). Noticeably, in the stomach, the number of viable *Lr*@GI was 2.4 times higher than that of *Lr*, indicating that *Lr*@GI exhibited enhanced resistance to the GIT. Meanwhile, the number of viable *Lr*@GI inside the small intestine, cecum, and colon was also obviously higher than that of *Lr* after oral administration (Fig. 3C), highlighting the substantial enhancement of *Lr* survival capacity in the GIT conferred by *Lr*@GI.

To further investigate the hydrolytic behaviour of GI in the GIT, GI hydrogel was placed into SGF and SIF for 2 h after incubation for infrared spectrum detection. Combined with Fig. 2D, it was observed that the absorption band of −OH stretching vibration of GI in SGF was concentrated at 3282.32 cm^{-1}, the absorption band of the −OH stretching vibration of GI in the SIF was shifted at 3414.57 cm^{-1}. Interestingly, GI hydrogel showed an

obvious absorption peak at 2930.84 cm^{-1} in SIF while disappeared in SGF, which might be due to the change of the C−H vibration frequency in GI hydrogel (Supporting Information Fig. S4). Additionally, to visualize the morphological changes and release of *Lr*@GI in the GIT, we performed simulated gastrointestinal fluid experiments by incubating *Lr* and *Lr*@GI in SGF and SIF. Morphological changes of *Lr* and *Lr*@GI in SGF and SIF were subsequently observed using SEM. The result was depicted in Fig. 3D, the cell walls of naked *Lr* underwent contraction and deformation in SGF, whereas the morphology of *Lr* remained largely unchanged in SIF. Following encapsulation in GI hydrogel, *Lr* maintained its morphology in both SGF and SIF, with evident hydrogel encapsulation, indicating that GI functions as a dynamic barrier "shield" enhancing the resistance of *Lr* to gastric acid. Further examination revealed that the hydrogel of *Lr*@GI in SIF was notably reduced compared to SGF, suggesting that GI, acting as a prebiotic, can be metabolized by intestinal probiotics upon entering the intestine, thereby promoting the release of *Lr*. Additional observations showed signs of the GI hydrogel did not surround the *Lr* as tightly in SIF compared to SGF, with most of the structure exhibiting significant cracking instead. This phenomenon might be attributed to the pH and ionic strength of intestinal fluid affecting the solubility of the GI hydrogel, as well as the continuous proliferation of bacteria, which may impact the extent of cracking. However, under alkaline conditions, the amino (NH_2) groups accept protons (H^+), altering their charge state and affecting the stability of intramolecular hydrogen bonds and other non-covalent bonds[80,81]. This weakens the intermolecular binding force of gelatin, facilitating their decomposition and thereby promoting the release of *Lr* in the intestine. Therefore, *Lr*@GI had stronger resistance to GIT, which laid a foundation for subsequent experiments.

Moreover, the specific primers targeting *Lr* was designed to verify its effective colonization at the tumor site[82]. The primer sequence was shown in Supporting Information Table S1. DNA was extracted from tissues for DNA gel electrophoresis, revealing that relevant sequences were expressed exclusively in tumor tissues from mice orally administered with *Lr* or *Lr*@GI (Supporting Information Fig. S5A and S5B). This further validated the ability of *Lr* to infiltrate the tumor site, possibly due to the hypoxic conditions within the tumor area. In comparison to normal surrounding tissue, the lower oxygen level in the tumor region provided a suitable environment for the proliferation of facultative and anaerobic bacteria. To further elucidate the *in situ* distribution of bacteria within the tumor, we administrated probiotics orally to CT26 orthotopic tumor mice, the result revealed that *Lr*@GI significantly accumulated at the tumor site, reaching a peak at 48 h, with a colony count higher than that of naked *Lr* (Fig. 3E and Supporting Information Fig. S6). In addition, similar results were obtained in the MC38 orthotopic tumor model (Supporting Information Fig. S7A−S7D). These findings offered the possibility of anti-tumor treatment with *Lr*@GI.

3.3. Biosafety assessment of synbiotic hydrogel capsules Lr@GI

The biosafety of the synbiotic hydrogel capsules *Lr*@GI was investigated through blood routine and blood biochemical tests. BALB/c mice were randomly allocated into four groups: PBS, GI, *Lr* and *Lr*@GI. Blood samples were collected from the orbital socket of mice at different time points, and the safety of bacterial treatment was evaluated by blood routine assessments. The results indicated that counts of white blood cell (WBC), red blood cell (RBC), and platelet (PLT) fell within normal ranges and did not exhibit statistically significant differences between groups at 7 days (Fig. 4A−C). Similarly, the levels alanine aminotransferase (ALT), aspartate aminotransferase (AST), and alkaline aminotransferase (ALP) exhibited similar results (Fig. 4D−F), suggesting that oral administration of *Lr* or *Lr*@GI did not induce any hepatic function impairment in mice. It is likely attributed to the benign nature of the selected gelatin, oligofructose and prebiotics for human consumption.

Impaired intestinal barrier function leads to increased permeability of the intestinal tract, allowing pathogens and toxins to enter the bloodstream through the damaged intestinal mucosa, resulting in various diseases[83,84]. Therefore, the integrity of the intestinal barrier is a crucial criterion for evaluating the safety of intestinal tissues. To assess the biosafety of *Lr*@GI in intestinal tissues, a fluorescent probe called FITC-Dextran was utilized for precise evaluation of intestinal permeability. Healthy mice were administered different formulations the day before the experiment. After fasting for 4 h the next day, each mouse received 200 μL (25 mg/mL) of FITC-Dextran solution by gavage and continued fasting for 3 h. As shown in Fig. 4G, there was no significant difference in fluorescence intensity among the other groups compared to the PBS group (Fig. 4H), indicating that the intestinal barrier function was intact and there was no leakage into the bloodstream. Furthermore, the tight junction protein zonula occludens-1 (ZO-1) plays a critical role in maintaining the integrity of the intestinal mucosal barrier and regulating intestinal permeability[85]. Therefore, the expression of ZO-1 in normal mice administered *Lr* and *Lr*@GI by oral gavage was examined. Western blot results showed in Fig. 4I that consistent expression levels of the intestinal barrier protein ZO-1 across all groups, suggesting that *Lr*@GI has good biocompatibility and does not cause significant damage to the intestinal tract. The aforementioned experimental results indicated that the synbiotic hydrogel capsules formed by prebiotics camouflaged with probiotics exhibited superior biosafety.

3.4. Study on the anti-tumor effect of synbiotic hydrogel capsules Lr@GI in vivo

As a common probiotic, *Lr* has been widely used in the research of various diseases, and its anti-tumor mechanisms are diverse[38]. Therefore, the anti-tumor efficacy of *Lr* and *Lr*@GI was investigated. Firstly, the safety of GI hydrogel was evaluated in a dose-dependent manner, as shown in Supporting Information Fig. S8A, even at the concentration of 2000 μg/mL, GI did not have any significant effect on CT26 cells, indicating that GI hydrogel was not cytotoxic to CT26 cells within a certain range. Secondly, we conducted a dose-dependent evaluation of *Lr* and *Lr*@GI *in vitro*. As shown in Fig. S8B, the cell viability gradually decreased with the increase of the dose of *Lr* and *Lr*@GI, when the concentration of *Lr* was 10^6−10^8 CFU/mL, the cell viability reached about 50%, and the therapeutic effects of *Lr* and *Lr*@GI were similar. Therefore, so we chose the dose of 10^6 CFU/mL for follow-up *in vitro* experiments. For the investigation of anti-tumor effect *in vivo*, the orthotopic colon cancer tumor model was established and mice were imaged *in vivo* on the eighth day of tumor growth. The successfully implanted tumor mice were randomly assigned into five groups: PBS, GI, *Lr*, *Lr* + GI, and *Lr*@GI. Here, the administration of diverse agents adhered to the schedule delineated in Fig. 5A, with treatments being delivered once every two days, totaling five

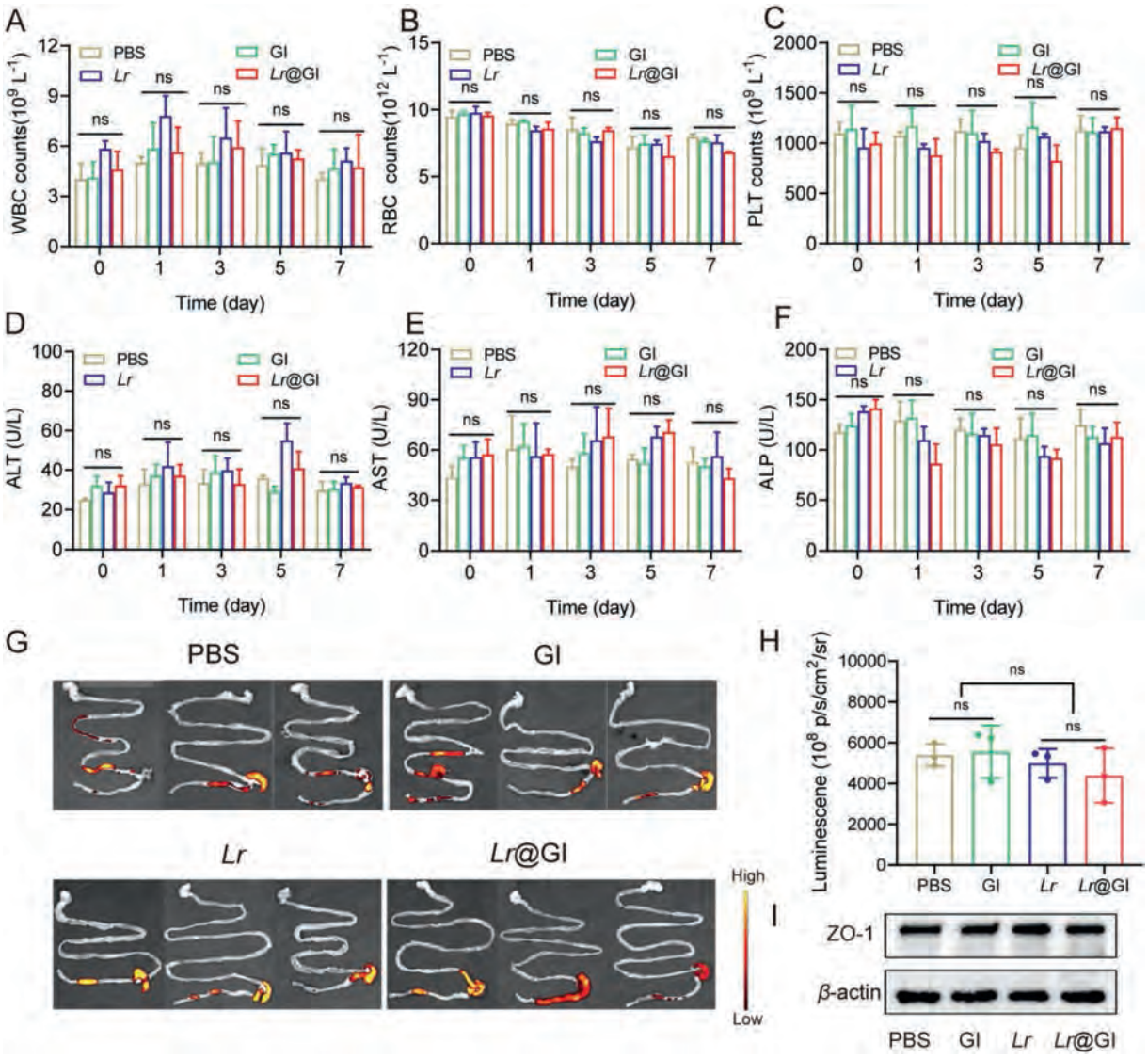

Figure 4 The safety assessment of *Lr*@GI in the GIT. Assessment of *in vivo* biological safety. PBS, GI, *Lr*, and *Lr*@GI (*Lr*, 100 μL, 1×10^8 CFU/mL) were administered orally by gavage and blood was withdrawn at the specified time points (Days 0, 1, 3, 5, and 7). (A−C) Routine blood analysis including WBC, RBC and PLT counts ($n = 3$). (D−F) ALT, ALP, and AST levels. ($n = 3$). Reference range of WBC count: 0.8×10^9−6.8×10^9/L, RBC count: 6.36×10^{12}−9.42×10^{12}/L, PLT count: 450×10^9−1590×10^9/L, ALT: 10.06−96.47 U/L, AST: 36.31−235.48 U/L, ALP: 22.52−474.35 U/L. (G) Fluorescence images of isolated intestine of mice in each group after administration of FITC-Dextran ($n = 3$). (H) The fluorescence quantitative results of isolated intestinal tract of mice administered FITC-Dextran in each group. (I) The expression level of ZO-1 protein in each group after administration of FITC-Dextran. Data are presented as mean ± SD ($n = 3$). ns, not significant.

sessions. Tumor distribution was assessed on Days 0, 5, 10, and 18 using IVIS, and tumor size was quantified based on fluorescence intensity (Fig. 5B). The relative fluorescence quantification as shown in Supporting Information Fig. S9A revealed that tumor volume amplification in the PBS group, while tumor volume in the GI and *Lr* groups either slightly decreased or remained unchanged. Particularly notable was the significant reduction in tumor volume observed in the *Lr*@GI group during treatment. After 20 days, the mice were euthanized, and the tumor tissues in each group were photographed and weighed, as depicted in Fig. 5C and D, the tumor weights of mice in various treatment groups, with the statistical results indicating that tumor weights in the GI and *Lr* groups were reduced compared to the PBS group. There was no significant difference between the GI and *Lr* groups, both of which demonstrated significant anti-tumor effects. This is likely due to GI, as a prebiotic, producing SCFAs with anti-tumor properties through microbial metabolism[86,87]. Notably, *Lr*@GI exhibited its most potent anti-tumor effect. In addition, the tumor morphology and cell death were evaluated by H&E and TUNEL staining after treatment, as shown in Fig. 5F. Minimal cell death was observed in the PBS group, while the *Lr*, GI, and *Lr* + GI groups exhibited partial cell death. The *Lr*@GI group displayed loose cellular arrangement, and nuclear consolidation was evident. What's more, the TUNEL staining also presented extensive necrosis in the *Lr*@GI group, suggesting that the *Lr*@GI group could effectively treat

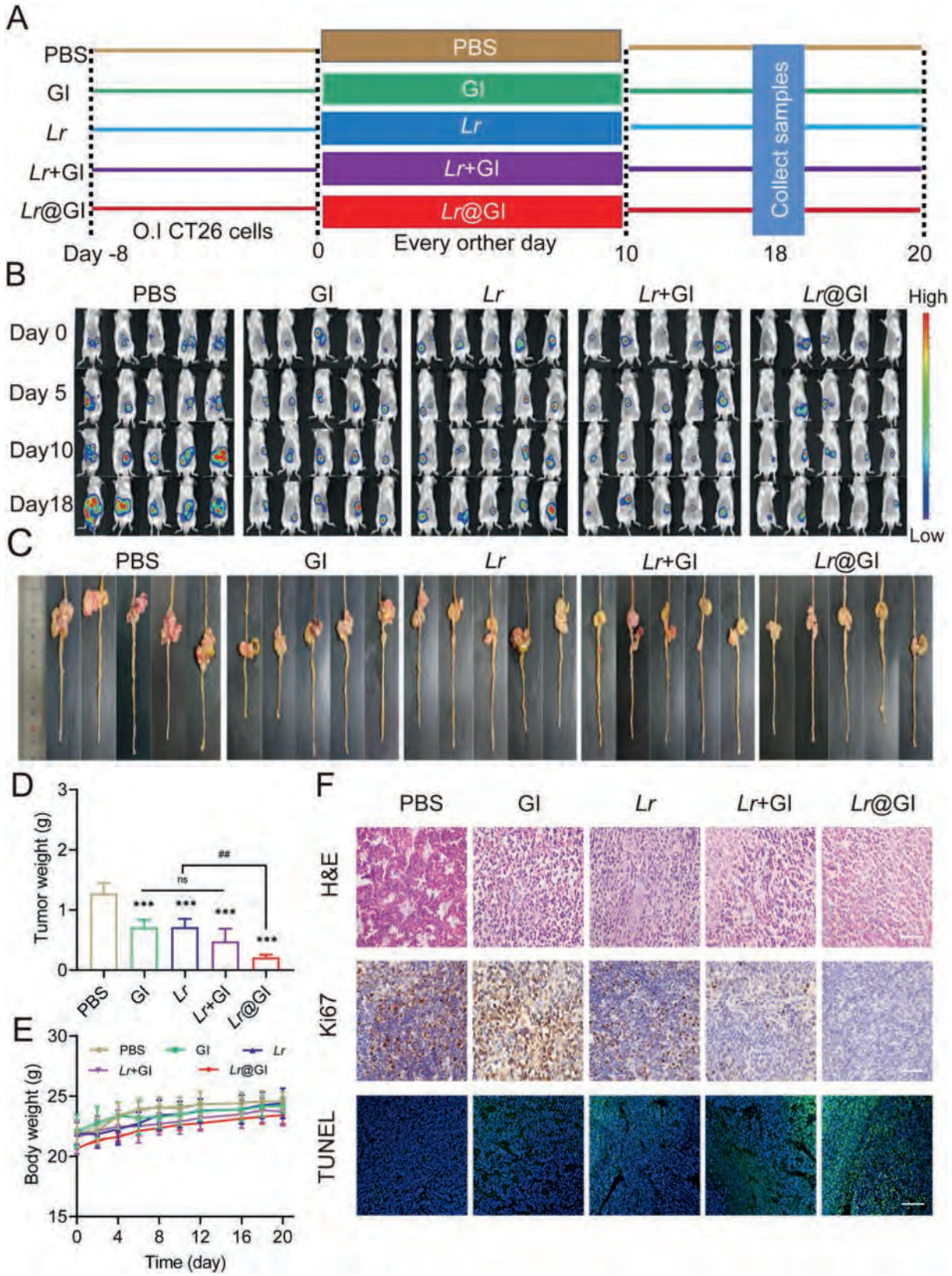

Figure 5 *In vivo* anti-tumor efficacy of synbiotic hydrogel capsules *Lr*@GI. (A) The schematic illustration of treatment protocols for orthotopic colon cancer tumor model. (B) IVIS images of mice of different treatment groups at Days 0, 5, 10, and 18. (C) Photographs of tumors removed from each group on Day 20 after treatment. (D) Tumor weight of mice in different treatment groups ($n = 5$). (E) Average body weight of mice during treatment. (F) H&E, Ki67, and TUNEL staining of the tumor tissue (scale bar = 50 μm). Data are presented as mean ± SD ($n = 5$). $^{***}P < 0.001$ *vs*, PBS, $^{\#\#}P < 0.01$ *vs*, *Lr*@GI. ns, not significant.

colon cancer. Ki67, primarily assessing tumor cell proliferation, showed reduced staining intensity in the *Lr*@GI group. More convincingly, as shown in Fig. S9B, we detected the changes of pro-apoptotic protein Bax and anti-apoptotic protein Bcl-2 in tumor tissue. The Bax/Bcl-2 ratio in the *Lr*@GI group was significantly increased compared with the other groups (Fig. S9C), indicating that *Lr*@GI had obvious anti-tumor efficacy. Furthermore, mice were weighed every 2 days, and no weight loss was observed following any of the treatments, indicating no serious systemic toxicity of *Lr*@GI (Fig. 5E). In addition, histopathologic analysis was performed to further assess biosafety. As illustrated in Supporting Information Fig. S10, the results showed no abnormalities in cell morphology or inflammatory reactions in the heart, liver, spleen, lung, and kidney. Overall, our findings suggested that *Lr*@GI demonstrates robust anti-tumor efficacy, potentially attributed to the prolonged *in vivo* retention of *Lr* facilitated by the "shield" GI.

3.5. Study on anti-tumor mechanism of synbiotic hydrogel capsules Lr@GI in vitro

Encouraged by the remarkable experimental results of *Lr*@GI in eradication of tumor cells *in vivo*, the anti-tumor effect mechanism of *Lr*@GI was further investigated *in vitro*. Initially, the cytotoxicity of *Lr*@GI on CT26 cells was evaluated by CCK-8 assay. As shown in Fig. 6A, the cytotoxicity of both *Lr* and *Lr*@GI on tumor cells exhibited similarity, with a cell death rate of approximately 40%. This indicated that the presence of GI as a shield for *Lr* did not compromise its anti-tumor efficacy. It has been reported that reuterin produced by *Lr* can induce apoptosis of colon cancer cells by glutathione (GSH) consumption[88]. Rapid GSH consumption inhibited the expression of the cofactor glutathione peroxidase 4, preventing the conversion of toxic peroxides to non-toxic hydroxyl compounds and activating intracellular oxidative stress[89]. Primarily, the change in intracellular GSH was explored. The result revealed no significant reduction in the GI group compared to the control group, while GSH levels were reduced to a similar extent in both the *Lr* and *Lr*@GI groups (Fig. 6B), suggesting that GI-camouflaged *Lr* did not impact GSH consumption. It has been demonstrated that tumor cells consistently maintain a redox balance to sustain rapid proliferation, and the consumption of GSH, as the principal cellular antioxidant, which disrupts the cellular redox balance, leading to an increase in peroxides[90]. Subsequently, 2′,7′-dichlorofluorescein diacetate (DCFH2-DA) was employed as a probe to further detect the changes of CT26 intracellular ROS, and the flow fluorescence intensity showed a significant increase in both *Lr* and *Lr*@GI, indicating that *Lr* or *Lr*@GI could increase ROS by depleting the CT26 intracellular GSH level to disrupt the redox balance (Fig. 6C). To visually confirm the alteration of ROS, fluorescence confocal microscopy was utilized to photograph the treated cells, with the results aligning with those obtained through flow cytometry (Fig. 6D). It has been reported that ROS can regulate the activation of NLRP3 inflammasome through various mechanisms, thereby participating in the occurrence and development of inflammatory responses and diseases[91]. To further corroborate this finding, immunoblotting experiments were performed to investigate the expression of NLRP3 in the treated groups. Encouragingly, both *Lr* and *Lr*@GI were found to activate NLRP3 expression (Fig. 6E), the corresponding protein quantification results depicted in (Supporting Information Fig. S11A). Meanwhile, the Bax/Bcl-2 ratio was elevated in *Lr* and *Lr*@GI compared with the control and GI groups (Fig. S11B), providing further evidence that *Lr* or *Lr*@GI induced apoptosis in CT26 cells. Numerous effectors of cell death have been identified to regulate the activation of the NLRP3 inflammasome through diverse pathways leading to cell death[92]. Mounting evidence suggested that NLRP3 could induce macrophage polarization towards M1 macrophages. For example, *A. Muciniphila* has been reported to inhibit colon cancer development by activating the TLR2/NLRP3 pathway mediating M1 macrophage activation[93]. To ascertain whether *Lr* induces M1 macrophages through the NLRP3 pathway, CT26 cells treated with *Lr* or *Lr*@GI were co-cultured with RAW264.7 cells, and macrophage polarization levels in RAW264.7 cells were examined. Flow cytometry results showed a significant increase in the ratio of M1/M2 in the *Lr* and *Lr*@GI groups, indicating that *Lr* and *Lr*@GI could induce M1 macrophage polarization (Fig. 6G and Supporting Information Fig. S12). An intimate relationship exists between macrophage polarization and ROS. ROS affects the direction of macrophages by participating in the activation of signaling pathways and regulation of transcription factors, thereby regulating the process of inflammatory response[94]. Immunofluorescence showed that macrophages treated with *Lr* or *Lr*@GI expressed higher ROS levels compared to control group (Fig. 6F and Fig. S11C). Furthermore, the co-culture of CT26 treated with *Lr* or *Lr*@GI with RAW264.7 revealed a significantly increase in the expression of tumor necrosis factor (TNF-α) and pro-inflammatory cytokine interleukin-1beta (IL-1β) (Fig. 6H and I). This suggested that M1 macrophage polarization could induce a robust anti-proliferative response, which might be beneficial for tumor cell regression. The above experimental results demonstrated that *Lr*@GI induced M1 macrophage polarization to exert antitumor effect by depleting GSH, leading to increased ROS levels, and simultaneously activating NLRP3 inflammasomes.

3.6. Study on the anti-tumor mechanism of Lr@GI in vivo

Having confirmed the compelling *in vivo* anti-tumor efficacy of *Lr*@GI *in vivo* and the elucidated anti-tumor mechanism *in vitro*, we further delved into understanding the anti-tumor mechanism of *Lr*@GI *in vivo*. Firstly, the GSH levels in tumor tissue from different treatment groups were detected, as depicted in Fig. 7A. Compared to the PBS and other treatment groups, the *Lr*@GI group exhibited a significantly reduction in GSH levels, indicating a substantial decrease in cellular antioxidant capacity post-treatment. Studies have established that maintaining the dynamic balance between the cellular redox capacity and oxidation levels is crucial, and a decrease in redox levels may disrupt this equilibrium, potentially inducing oxidative stress[95]. Subsequently, the level of ROS in the tumor tissue was measured by dihydroethidium (DHE), which emits red fluorescence upon oxidation. As described in Fig. 7B, no significant red fluorescence was detected in the PBS group, while a slight red fluorescence was observed in the *Lr* group, indicating the production of a small amount of ROS. Notably, the *Lr*@GI group exhibited the most intense red fluorescence compared to the *Lr* + GI group, as shown in the relative fluorescence quantification of ROS in Supporting Information Fig. S13A. These results suggested that *Lr*@GI had the ability to perturb the oxidative balance and generate ROS by depleting GSH, thereby inducing oxidative stress in tumor cells. Crucially, elevated ROS levels could trigger the activation of NLRP3 inflammasome[96]. Therefore, Western blot was conducted to assess the expression of NLRP3 protein across different

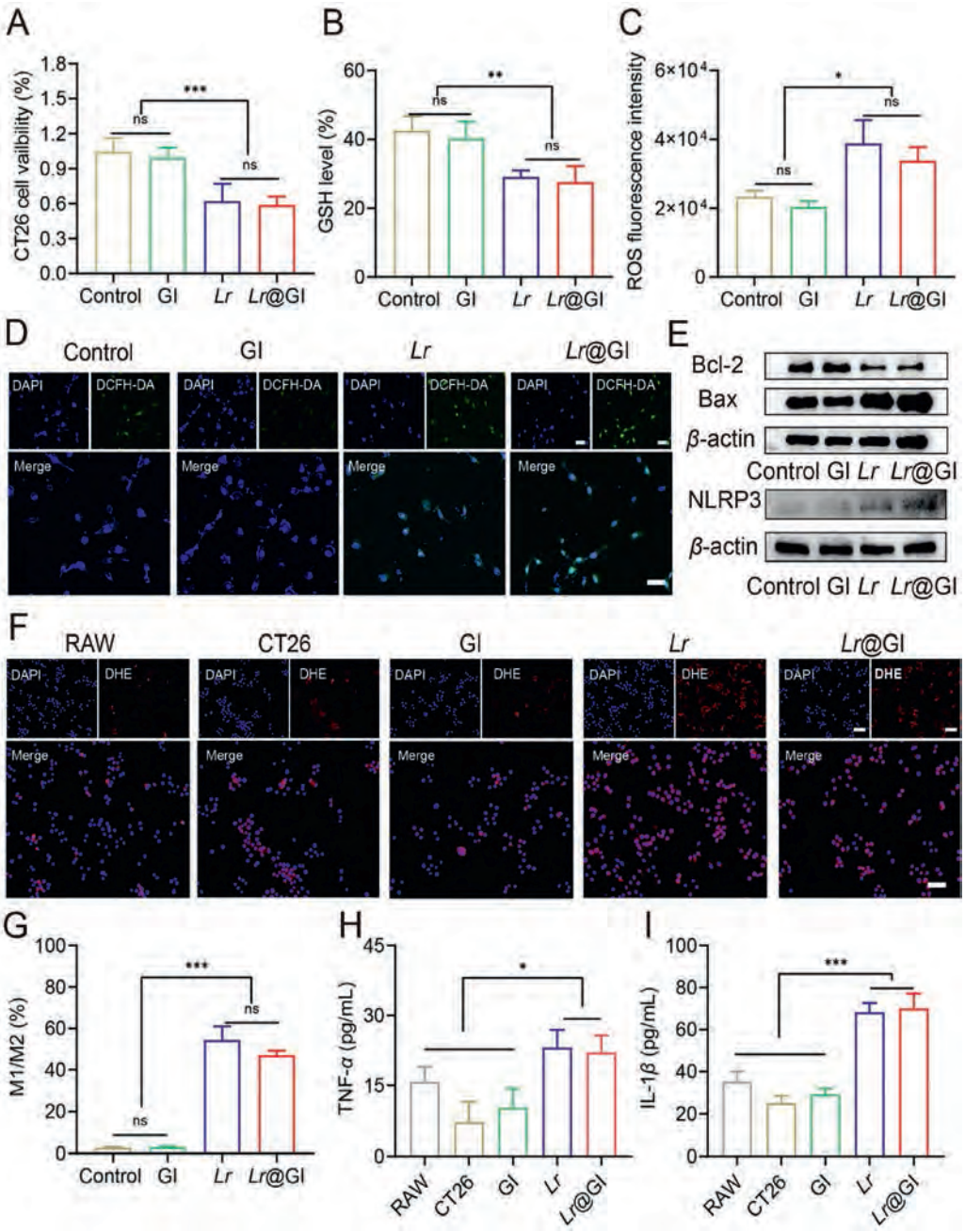

Figure 6 The anti-tumor mechanism of synbiotic hydrogel capsules *Lr*@GI *in vitro*. (A) Cytotoxicity detection of CT26 cells with different treatment groups by CCK-8. (B) GSH levels of CT26 cells in different treatment. (C) The ROS of CT26 cells were detected by flow cytometry. (D) Immunofluorescence images of ROS expression in CT26 cells in different treatment groups (scale bar = 50 μm). (E) Expression of Bcl-2, Bax, and NLRP3 in CT26 cells. (F) Immunofluorescence images of ROS expression in RAW267.4 cells in different treatment groups (scale bar = 50 μm). (G) The M1/M2 ratio of macrophages in CT26 was measured by flow cytometry. The contents of (H) TNF-α and (I) IL-1β in RAW 264.7 cells in different treatment groups were detected by ELISA. Data are presented as mean ± SD (n = 3). *P < 0.05, **P < 0.01, ***P < 0.001. ns, not significant.

treatments. Results depicted in Fig. 7C and Fig. S13B revealed a significant increase in the expression level of NLRP3 in *Lr*@GI group, indicating the evident activation of the inflammatory response by *Lr*@GI *in vivo*. The activation of NLRP3 inflammasome was known to be involved in macrophage polarization, which played a pivotal role in the anti-tumor process[93]. Macrophages are widely distributed in the tumor microenvironment and serve various functions, including clearing dead tumor cells, regulating immune responses, and participating in tissue repair[97,98]. M1 macrophages predominantly exhibit anti-tumor activity in tumor immunity by secreting proinflammatory cytokines and toxic intermediates, thereby killing tumor cells and inhibiting tumor growth[99]. To further investigate whether the mechanism underlying the superior anti-tumor effect of *Lr*@GI

was related to macrophage polarization, flow cytometry was employed to quantify macrophage polarization in the tumor. The results revealed that the expression of CD86, a marker of M1 macrophages, was significantly higher in the *Lr* + GI and *Lr*@GI groups compared to the PBS group (Fig. 7D). In contrast, the expression of CD206, a marker of M2 macrophages, was lower, indicating a polarization of macrophages toward the anti-tumor M1 macrophages after treatment. Furthermore, the analysis of the M1 to M2 ratio revealed no significant change in the M1/M2 ratio between the GI group and the PBS group (Fig. S13C). However, the ratio of M1/M2 increased in other treatment groups, notably reaching approximately 0.15, 2.85, and 9.15 in the *Lr*, *Lr* + GI, and *Lr*@GI groups, respectively. Particularly in the *Lr*@GI treatment group, there was a significant increase in the M1/M2 ratio, indicating that *Lr*@GI treatment effectively promotes the polarization of tumor-associated macrophages (TAMs) from M2 phenotype to M1 phenotype, thereby exerting an anti-tumor effect. M1 macrophages, often termed "classically activated" or "pro-inflammatory" are activated in response to infection or inflammation. These cells produce high levels of inducible nitric oxide synthase (iNOS), which generates nitric oxide (NO), essential for pathogen elimination and the regulation of inflammatory responses. Thus, iNOS is considered a characteristic protein of M1 macrophages[100]. On the other hand, M2 macrophages, known as "alternatively activated" or "anti-inflammatory", play roles in tissue repair, immunomodulation, and anti-tumor activity. These cells typically express arginase, arginase was recognized as a characteristic protein of M2 macrophages[101]. We also assessed the expression of macrophage polarization-associated proteins iNOS and Arginase in tumor tissue, and the results in Fig. 7C showed that the expression of iNOS was elevated in the *Lr*@GI group, and that the expression of Arginase was decreased compared with the other groups. The relative protein quantification of iNOS and Arginase were shown in Fig. S13D and S13E. Both immunofluorescence and immunohistochemistry demonstrated that *Lr*@GI promoted the increase of iNOS in the tumor tissue (Fig. 7E and F), both the relative fluorescence intensity and the relative quantification of iNOS were shown in Fig. S13F and S13G, suggesting that macrophages polarized into the M1 macrophages, contributing to anti-tumor effect. Polarized M1 macrophages release inflammatory mediators, including cytokines and oxidative free radicals, regulating the inflammatory response and influencing the survival, proliferation and invasion of tumor cells[102]. To examine the impact on the inflammatory response, we assessed changes in the relevant pro-inflammatory cytokines IL-1β and TNF-α in tumor from different treatment groups. As illustrated in Fig. 7G and H, significantly higher cytokine expression was observed in the *Lr*@GI group compared to PBS and the other treatment groups, indicating that *Lr*@GI-induced M1 macrophages polarization may promote anti-inflammatory responses and exert anti-tumor effect.

Furthermore, the tight junction protein ZO-1 plays a crucial role in maintaining the integrity of intestinal mucosal barrier and regulating intestinal permeability[103,104]. The visual examination of immunohistochemistry results revealed a significant increase in ZO-1 expression in *Lr*@GI group compared to the PBS group (Fig. 7I), the relative quantification depicted in Fig. S13H. Meanwhile, the Western blot analysis yielded consistent experimental result (Fig. 7J), the semi-quantitative protein results are shown in Fig. S13I. These findings suggested that *Lr*@GI treatment could effectively regulate intestinal barrier function, which was essential for preventing microbial invasion and maintaining immune balance.

3.7. Study on effect of Lr@GI on intestinal flora and the anti-tumor effect of Lr@GI collaborates with 5-FU

Mounting evidence from both preclinical and clinical studies implicates the gut microbiota as a key player in the progression of colon cancer[105]. Emboldened by the remarkable therapeutic efficacy of *Lr*@GI presented in the above section. Subsequently, we explored whether *Lr*@GI treatment could reshape the dysbiosis of gut microbiota in mouse model of colon cancer and thus cease the progression of the disease. Therefore, to assess the impact of *Lr*@GI on the changes in intestinal flora in mice with colon cancer, 16S rDNA amplicon sequencing was performed on fecal samples. Microbial β diversity reflects differences in microbial diversity among different groups. Based on the abundance information of ASV/OTU in the samples, the sample difference distance matrix was obtained through the Jaccard distance algorithm. The principal coordinate analysis, depicted in Fig. 8A, revealed clear separation between groups, indicating significant variations in the composition of intestinal flora among different treatment groups. Additionally, at the family level, the abundance of *Lactobacillaceae* and *Rikenellaceae* in the *Lr*@GI group were increased, which were known to produce propionic acid and butyric acid from substrates such as succinate, lactate, or acetate (Fig. 8B). At the phylum level, the relative abundance of *Lactobacillus* and *Firmicutes* were enriched, while the relative abundance of *Actinobacillu*s were reduced in the *Lr*@GI group compared to the PBS group (Fig. 8C−E). At the species level, the results demonstrated that compared with PBS group, the *Lr*@GI-treated group exhibited increased abundance of *Lactobacillus johnsonii*, *Muribaculaceae*, *Lactobacillus*, and *Prevotellaceae* (Supporting Information Fig. S14). These probiotics are known to elevate SCFAs levels[106-108] with *Muribaculaceae* and *Prevotellaceae* particularly associated with promoting butyrate production[109,110]. These results suggested that *Lr*@GI may indirectly promote butyrate production by regulating intestinal flora to increase the abundance of probiotics. Inulin, as a polysaccharide, could be metabolized by intestinal microbiota to produce a large amount of SCFAs, inducing immune responses and exhibiting anti-tumor effect[111,112]. Moreover, while it has been reported that the main metabolites of *Lr* include reuterin and lactic acid and SCFAs[38,39,113], there is currently no direct evidence demonstrating whether *Lr* directly produces butyric acid. To investigate whether *Lr*@GI can produce butyric acid *in vitro*, *Lr* and *Lr*@GI were incubated in MRS medium for 24 h, and the supernatant was collected. The content of SCFAs (acetic acid, propionic acid, isobutyric acid, butyric acid, isovaleric acid, valeric acid, and hexanoic acid) in the supernatant of MRS, *Lr* and *Lr*@GI groups were detected by ELISA and mass spectrometry, as depicted in Supporting Information Fig. S15A and S15B. The results indicated that both *Lr* and *Lr*@GI did not produce butyrate *in vitro* but rather increased acetate production (Fig. S15C−S15I). It has been reported that the production of *B. pseudobacterium* has a protective effect on non-alcoholic fatty liver disease-associated hepatocellular carcinoma through the secretion of acetate[114]. Subsequently, fecal samples from mice in different treatment groups were analyzed using mass spectrometry, revealing the

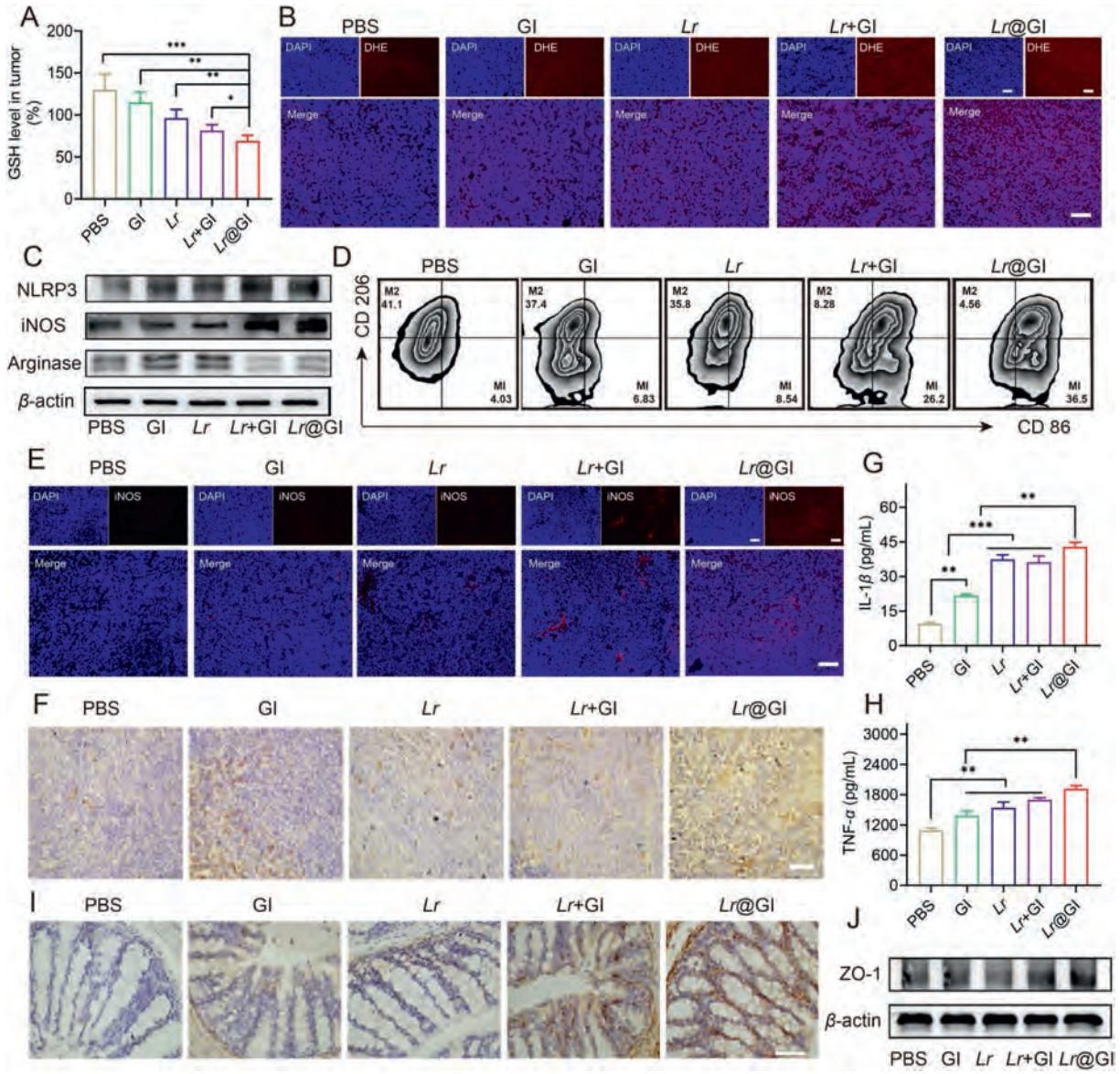

Figure 7 Anti-tumor mechanism of synbiotic hydrogel capsules *Lr*@GI *in vivo.* (A) The level of GSH expression in tumor. (B) Immunofluorescence image of ROS expression in tumor (scale bar = 50 μm). (C) The protein expression of NLRP3, iNOS, and Arginase in different treatment groups. (D) The representative flow cytometric plots of CD86 and CD206 in different treatment groups. (E) Immunofluorescence images and (F) Immunohistochemical images of iNOS in tumor (scale bar = 50 μm). (G) The tumor related cytokines expression of IL-1β and (H) TNF-α. (I) Histochemical images of ZO-1 protein in different treatment groups (scale bar = 20 μm). (J) The Western blot results of ZO-1 protein in different treatment groups ($n = 3$). Data are presented as mean ± SD ($n = 3$). *$P < 0.05$, **$P < 0.01$, ***$P < 0.001$.

levels of 7 fatty acids as presented in Fig. 8F. The levels of 7 SCFAs in *Lr*@GI and health groups were higher than in the other treatment groups (Fig. 8G). Although no significant changes in the content of acetate, propionate, and butyrate were observed in the *Lr*, GI, and *Lr* + GI groups compared to the PBS group, the content of the three SCFAs in *Lr*@GI was significantly increased and returned to normal levels (Fig. 8H–J). Notably, this increase was attributed not only to elevated acetate levels but also to an augmentation in butyrate content. This result suggested that *Lr*@GI may indirectly enhance butyrate production by modulating the intestinal microbiota balance and enriching other butyrate-producing bacteria. To further elucidate the anti-tumor effect of SCFAs *in vitro*, butyrate, acetate, and propionate were selected for cytotoxicity experiments on CT26 cells. Results from the CCK-8 toxicity assay showed that all three SCFAs could promote the apoptosis of CT26 cells (Supporting Information Fig. S16A–S16C). The expression of relevant apoptotic protein was detected by Western blot (Fig. S16D–S16F). The results revealed an increased Bax/Bcl-2 ratio following treatment with the three SCFAs (Fig. S16G–S16I), indicating that SCFAs could inhibit the proliferation of colon cancer cells. The aforementioned results suggested that *Lr*@GI not only regulated intestinal flora and increased the abundance of beneficial bacteria, but also produced abundant SCFAs to exert an anti-tumor effect.

5-FU (5-fluorouracil), a derivative of uracil, has been a classic and standard chemotherapy agent for the treatment of colon

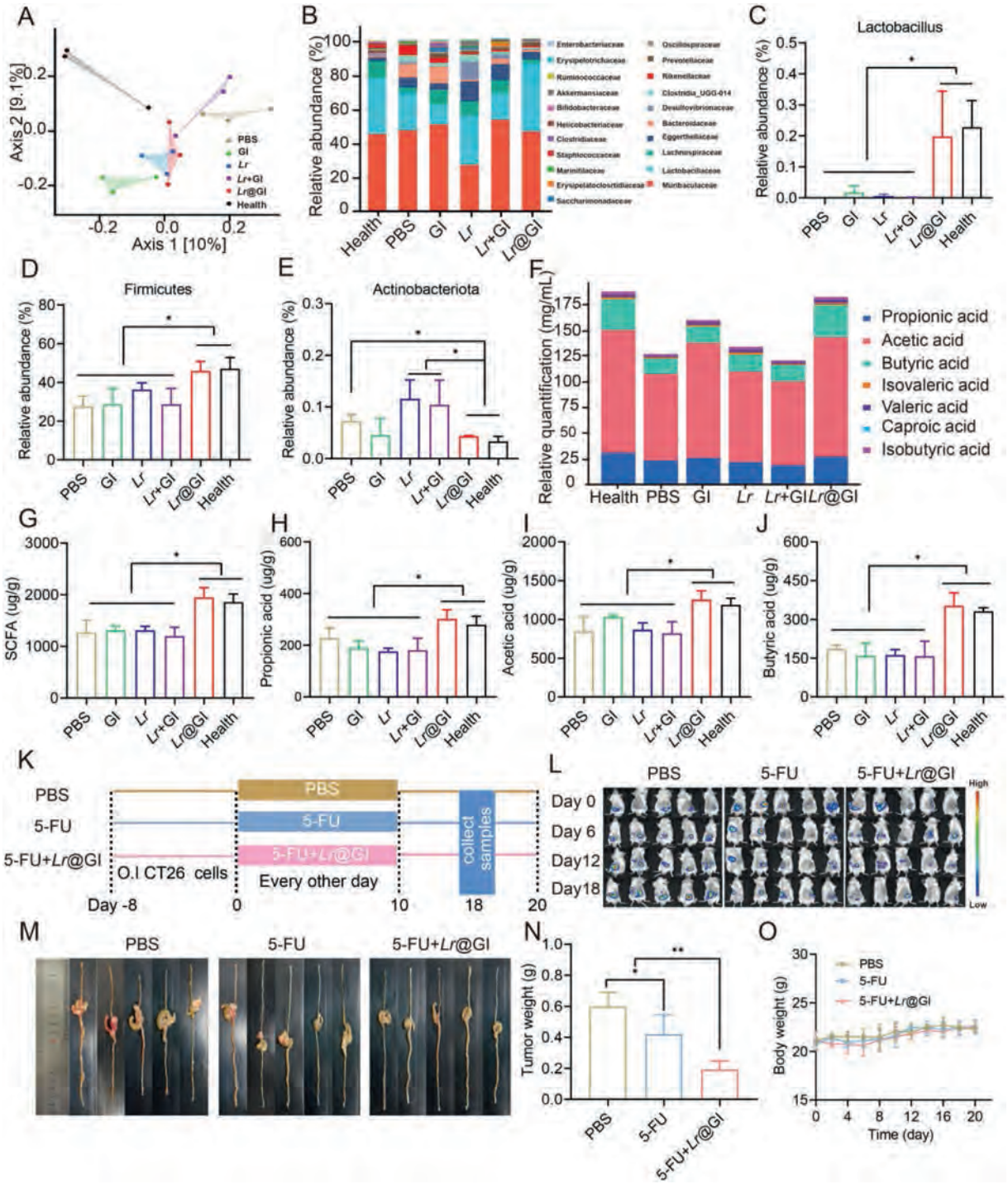

Figure 8 Changes of intestinal flora and SCFAs *in vivo* and enhancement of the anti-tumor effect of *Lr*@GI collaborates with 5-FU. (A) The PCoA analysis of β diversity in intestinal microbes ($n = 3$). (B) The species distribution at family level in different treatment groups. The expression of (C) *Lactobacillus*, (D) *Firmicutes*, and (E) *Actinobacteria* in different treatment groups. (F) Levels of SCFAs in different treatment groups ($n = 3$). (G) Expression of total SCFAs in different treatment groups. The expression of (H) propionic acid, (I) acetic acid, (J) butyric acid in different treatment groups. (K) The diagram of experimental design diagram. (L) IVIS images of mice in different treatment groups on Days 0, 6, 12, and 18. (M) Photographs of tumors removed from each group on Day 20 after treatment. (N) Tumor weight of mice during treatment ($n = 5$). (O) Average body weight of mice after 20 days with different treatment groups. Data are presented as mean ± SD ($n = 3$). $^{*}P < 0.05$, $^{**}P < 0.01$, $^{***}P < 0.001$.

cancer[115]. However, the clinical benefits of 5-FU are limited by drug resistance in colorectal tumor cells and common adverse side effects, such as gastrointestinal reactions[116]. Consequently, there is a pressing need to devise novel strategies to minimize or prevent adverse reactions of 5-FU and enhance treatment efficiency. Probiotics have been identified as a potential factor in reducing the risk of colon cancer[117]. Clinical reports indicate significant advantages of probiotics in patients with colon cancer undergoing 5-FU adjuvant therapy post-surgery[118]. Probiotics supplementation may confer anti-tumor effects, diminishing abnormal crypt formation, ameliorating tumor malignancy, and augmenting the apoptosis-inducing capability of 5-FU[119]. Given the potential anti-tumor properties of probiotics, their combination with conventional colon cancer therapies presents a plausible and safe strategy to enhance the therapeutic effectiveness of 5-FU through *Lr*@GI. Therefore, we conducted additional experiments to validate the anti-tumor efficacy of *Lr*@GI in combination with 5-FU *in vitro*. First, the cytotoxic effects of different doses of 5-FU on CT26 tumor cells were detected by CCK-8. As shown in Supporting Information Fig. S17A. The cytotoxic effect of 5-FU on CT26 cells was dose-dependent. Based on these results, a concentration of 100 μmol/L 5-FU was selected for subsequent experiments. To investigate the anti-tumor effect of 5-FU combined with *Lr*@GI, the CCK-8 result was shown in Fig. S17B. Compared to the control group, the viability of CT26 cells was significantly reduced in the treatment groups, with the inhibition rate of 5-FU and *Lr*@GI demonstrating similar effects, however, the combination group (5-FU + *Lr*@GI) exhibited a markedly greater reduction in cell viability. In addition, at the protein level, the anti-tumor efficacy was futher verified by detecting related apoptosis proteins. The Western blot results in Fig. S17C revealed that compared with the control group, the Bax/Bcl-2 ratio was increased in the 5-FU and *Lr*@GI groups, with no significant difference, indicating that 5-FU exhibit an anti-tumor effect to some extent. Furthermore, the Bax/Bcl-2 ratio was increased more significantly in the 5-FU + *Lr*@GI group (Fig. S17D), demonstrating that *Lr*@GI markedly enhanced the anti-tumor effect of 5-FU. To corroborate this conjecture *in vivo*, mice with successfully implanted CT26 orthotopic tumor mice were randomly divided into 3 groups: PBS, 5-FU, and 5-FU + *Lr*@GI. The experimental procedure was illustrated in Fig. 8K. The mice received treatments once every two days for a total of five treatments. Tumor distribution was assessed on Days 0, 6, 12, and 18 by IVIS equipment, and tumor size was determined based on fluorescence intensity (Fig. 8L). The results revealed an increase in tumor volume in the PBS group, a slight decrease in tumor volume in the 5-FU group, notably, a significant reduction in tumor volume observed in the 5-FU + *Lr*@GI group throughout the treatment period. After 20 days, the mice were euthanized, and the tumor tissues in each group were photographed and weighed, as depicted in Fig. 8M and N. These results were consistent with those in Fig. 8L, showing a decrease in tumor volume and weight in the treatment groups compared to the PBS group, with the most significant reduction observed in the 5-FU + *Lr*@GI group. These results suggested that *Lr*@GI could serve as an adjunctive treatment to enhance the efficacy of 5-FU as a chemotherapy agent for colon cancer. Furthermore, mice were weighed every 2 days, and no weight loss was observed following any of the treatments (Fig. 8O). It implied that *Lr*@GI represent a promising strategy to further enhance the therapeutic efficacy of 5-FU within a safe manner. These results laid the groundwork for the clinical translation of *Lr*@GI.

4. Discussion

Colon cancer stands as the most prevalent malignancy in the GIT, characterized by a heterogeneous process influenced by genetic and environmental factors[120]. Drug chemotherapy, primarily utilizing fluorouracil (5-FU), represents a cornerstone in the treatment for advanced colon cancer patients[121]. However, chemotherapy drugs not only kill tumor cells, but also inflict damage on normal cells, leading to intestinal toxicity and intricate alterations in the intestinal flora. This significantly diminishes the quality of life and therapeutic effectiveness for patients[122]. Consequently, the quest for a dependable, effective, and safe anti-tumor drug has ascended to a paramount position in contemporary research. Probiotic therapy emerges as a promising avenue for colon cancer, positioned at the forefront of precise and personalized treatment[93,123-125]. However, oral therapy encounters limitations concerning low bioavailability, insufficient gastrointestinal retention, and challenges in achieving significant cancer treatment effect using probiotics alone. Therefore, innovative approaches are being developed to enhance the competitiveness of probiotics in the pathological microenvironment, facilitating efficient probiotic colonization.

However, in the challenging GIT, the key to effectively treating colon cancer lies in improving the intestinal colonization and survival rate of *Lr*. In our study, a shield "GI" hydrogel based on the cross-linked hydrogen bond of prebiotic inulin and natural polymer gelatin was synthesized and coated with *Lr* synthetic synbiotic hydrogel capsules (*Lr*@GI). Bacterial viability experiments confirmed that GI had no significant impact on the growth and viability of *Lr*. Moreover, the GI shield hydrogel exhibited superior gastrointestinal retention properties, possibly attributed to the inherent high viscosity of inulin as a polysaccharide. Subsequently, we delved into the anti-tumor mechanisms of *Lr*@GI *in vivo* and *in vitro*. Previous research has reported that reuterin produced by *Lr* can induce apoptosis of colon cancer cells by depleting GSH, thereby disrupting the intracellular redox balance and triggering oxidative stress response[38]. The results of *in vivo* and *in vitro* experiments demonstrated that *Lr*@GI significantly consumed GSH, leading to a substantial release of ROS and an increased Bax/Bcl-2 ratio expression. Further exploration into the molecular mechanisms of cell death revealed that cell death effectors could regulate the activation of the NLRP3 inflammasome, leading to cell death through various pathways[92]. It has been reported that oxidative stress can affect the transcription level of NLRP3 through NF-κB and other transcription factors (SOD, Nrf2, AP-1)[126-128]. The accumulation of ROS also promoted the transcriptional activation of NLRP3, thereby increasing the expression levels of NLRP3 *in vivo* and *in vitro*, which can further influence the occurrence and development of tumors. After initiation, NLRP3 assembles the NLRP3 inflammasome, and cleaves pro-IL-1β to generate IL-1β[129,130], which might further enhance the pro-inflammatory characteristics of M1 macrophages and promote the clearance of tumor cells.

Moreover, the tight junction protein ZO-1 was vital for maintaining the integrity of intestinal mucosal barrier and controlling intestinal permeability[103]. Our study revealed that *Lr*@GI effectively elevated ZO-1 expression in colon tissue, indicating its potential to restore intestinal barrier function. Oral probiotics can regulate the composition of intestinal flora. Results from 16S rDNA sequencing revealed that *Lr*@GI could restore microbiota imbalance induced by colon cancer by modulating the intestinal microbiota. SCFAs are primarily produced in the intestine, with

most being absorbed by colonic epithelial cells through monocarboxylate transporters to provide energy for these cells or enter the bloodstream to participate in systemic metabolic regulation[131,132]. In contrast, SCFAs present in feces represent unabsorbed SCFAs that are ultimately excreted. These not only reflect the end products of microbial fermentation but also provide insight into the composition and fermentation capacity of the intestinal microbiota. Our result suggested that *Lr*@GI generates the most SCFAs in the intestinal tract, while fewer SCFAs may be produced in the *Lr*, GI, and *Lr* + GI groups, as they were likely absorbed by colonic epithelial cells, resulting in no significant differences in fecal SCFA levels. By detecting the supernatant of the medium *in vitro*, we found that the supernatant containing *Lr* could produce a large amount of acetic acid, which is a very interesting phenomenon. The anti-tumor effect of SCFAs has also been further demonstrated *in vitro*, although it has been shown that high doses of SCFAs, such as butyric acid and propionic acid could inhibit the anti-tumor effect blocked by CTLA-4 blockers[133]. It is important to note that SCFAs have variety physiological functions and benefits, including providing energy, regulating electrolyte balance, and protecting the intestinal mucosal barrier[134,135]. Additionally, the anti-tumor mechanism of SCFAs may be complex and require comprehensive consideration of the impact of other factors.

In clinical studies of colon cancer, 5-FU is considered the standard chemotherapeutic drug for the treatment of colon cancer[121]. In palliative care, 5-FU has a remarkable effect in relieving symptoms, improving quality of life, and prolonging life[136]. However, it is limited due to adverse reactions such as diarrhea, nausea and vomiting during chemotherapy[137]. The overall effective rate needs to be improved. Clinical reports have indicated that administration of probiotics significantly improves tumor malignancy and enhances apoptosis-inducing capacity of 5-FU in colon cancer patients receiving postoperative adjuvant 5-FU therapy[119,138]. Considering the anti-tumor properties of probiotics, enhancing the efficacy of 5-FU treatment with *Lr*@GI is a safe and feasible strategy. Our experimental findings additionally showcased the capacity of *Lr*@GI to augment the anti-tumor effect of 5-FU, potentially attributed to capability of *Lr*@GI to generate SCFAs, modulate intestinal flora, and enhance the tolerance of organism to chemotherapeutic drug. Therefore, the concurrent administration of *Lr*@GI and 5-FU serves as a valuable paradigm for microbial therapy aimed at bolstering the clinical efficacy of chemotherapeutic drug.

5. Conclusions

Colon cancer is a malignant tumor originating from the mucosal epithelium of the colon, which is one of the common malignant tumors of the digestive tract. The main objective of this article is to synthesize synbiotic hydrogel capsules encapsulated with probiotic *Lr* based on modified prebiotic "shield", named *Lr*@GI, for the treatment of colon cancer. Which demonstrated notable resistance to the challenging conditions of the GIT, thereby enhancing the bioactivity of probiotics *in vivo*. This was attributed to GI acting as a shield, prolonging the retention capacity of *Lr* in the GIT. Through comprehensive *in vivo* and *in vivo* experiments, we substantiated the therapeutic potential of *Lr*@GI. The straightforward processing involved in GI shield holds promise for streamlining the clinical implementation of probiotic therapy. This study unveiled that the synergistic application of *Lr*@GI with 5-FU could amplify anti-tumor efficacy with certain safety and practical benefits. Nevertheless, several limitations in this study necessitate further exploration. Firstly, the effectiveness and safety profile of *Lr*@GI should be evaluated in larger animal models or in patients with colitis. Secondly, it is imperative to ascertain whether *Lr*@GI can mitigate the clinical toxicity associated with existing drugs. As we continue to refine and advance this approach, *Lr*@GI holds the potential to pave the way for personalized medicine and open new avenues in the clinical translation of probiotics.

Acknowledgments

This work was financially supported by the National Natural Science Foundation of China (32172894), Academic Leaders Training Program of Pudong Health Committee of Shanghai (Grant No. PWRd2022-09), and the Scientific Research Project of Shanghai Pudong Hospital (YJYJRC202106).

Author contributions

Yang Wang and Xiaomin Su contributed to the design, performed experiments of the work and wrote the manuscript; Yao Liu and Lina Hu contributed to the acquisition of the work, performed statistical analysis; Lin Kang revised the article; Ce Xu, Zanya Sun and Chenyu Sun contributed to the conception of the work and provided project supervision. All authors have read and approved the final manuscript.

Conflicts of interest

The authors have no conflicts of interest to declare.

Appendix A. Supporting information

Supporting information to this article can be found online at https://doi.org/10.1016/j.apsb.2025.05.040.

References

1. O'Keefe SJD. Diet, microorganisms and their metabolites, and colon cancer. *Nat Rev Gastroenterol Hepatol* 2016;**13**:691−706.
2. Janney A, Powrie F, Mann EH. Host−microbiota maladaptation in colorectal cancer. *Nature* 2020;**585**:509−17.
3. Gomes AC, Hoffmann C, Mota JF. The human gut microbiota: metabolism and perspective in obesity. *Gut Microbes* 2018;**9**: 308−25.
4. Park EM, Chelvanambi M, Bhutiani N, Kroemer G, Zitvogel L, Wargo JA. Targeting the gut and tumor microbiota in cancer. *Nat Med* 2022;**28**:690−703.
5. Sanders ME, Merenstein DJ, Reid G, Gibson GR, Rastall RA. Probiotics and prebiotics in intestinal health and disease: from biology to the clinic. Nat Rev *Gastroenterol Hepatol* 2019;**16**: 605−16.
6. Li Q, Chan H, Liu WX, Liu CA, Zhou Y, Huang D, et al. *Carnobacterium maltaromaticum* boosts intestinal vitamin D production to suppress colorectal cancer in female mice. *Cancer Cell* 2023;**41**: 1450−65.e8.
7. Sugimura N, Li Q, Chu ESH, Lau HCH, Fong W, Liu W, et al. *Lactobacillus gallinarum* modulates the gut microbiota and produces anti-cancer metabolites to protect against colorectal tumourigenesis. *Gut* 2021;**71**:2011−21.

8. Xu H, Luo H, Zhang J, Li K, Lee MH. Therapeutic potential of *Clostridium butyricum* anticancer effects in colorectal cancer. *Gut Microbes* 2023;**15**:2186114.
9. Ghosh S, Singh R, Vanwinkle ZM, Guo H, Vemula PK, Goel A, et al. Microbial metabolite restricts 5-fluorouracil-resistant colonic tumor progression by sensitizing drug transporters *via* regulation of FOXO3−FOXM1 axis. *Theranostics* 2022;**12**:5574−95.
10. Qiao JY, Zeng RY, Chen QW, Zheng D, Hao PL, Liu XH, et al. Autonomously assembled living capsules by microbial coculture for enhanced bacteriotherapy of inflammatory bowel disease. *Nano Lett* 2023;**23**:4375−83.
11. Zhou J, Li M, Chen Q, Li X, Chen L, Dong Z, et al. Programmable probiotics modulate inflammation and gut microbiota for inflammatory bowel disease treatment after effective oral delivery. *Nat Commun* 2022;**13**:3432.
12. Cao Z, Wang X, Pang Y, Cheng S, Liu J. Biointerfacial self-assembly generates lipid membrane coated bacteria for enhanced oral delivery and treatment. *Nat Commun* 2019;**10**:5783.
13. Li Z, Behrens AM, Ginat N, Tzeng SY, Lu X, Sivan S, et al. Biofilm-inspired encapsulation of probiotics for the treatment of complex infections. *Adv Mater* 2018;**30**:e1803925.
14. Luo R, Chang Y, Liang H, Zhang W, Song Y, Li G, et al. Interactions between extracellular vesicles and microbiome in human diseases: new therapeutic opportunities. *iMeta* 2023;**2**:e86.
15. Liu Y, Lu Y, Ning B, Su X, Yang B, Dong H, et al. Intravenous delivery of living listeria monocytogenes elicits gasdermin-dependent tumor pyroptosis and motivates anti-Tumor immune response. *ACS Nano* 2022;**16**:4102−15.
16. Yaghoubi A, Khazaei M, Avan A, Hasanian SM, Soleimanpour S. The bacterial instrument as a promising therapy for colon cancer. *Int J Colorectal Dis* 2020;**35**:595−606.
17. Ooijevaar RE, Terveer EM, Verspaget HW, Kuijper EJ, Keller JJ. Clinical application and potential of fecal microbiota transplantation. *Annu Rev Med* 2019;**70**:335−51.
18. Minkoff NZ, Aslam S, Medina M, Tanner-Smith EE, Zackular JP, Acra S, et al. Fecal microbiota transplantation for the treatment of recurrent *Clostridioides difficile* (*Clostridium difficile*). *Cochrane Database Syst Rev* 2023;**4**:Cd013871.
19. Clairmont C, Lee KC, Pike J, Ittensohn M, Low KB, Pawelek J, et al. Biodistribution and genetic stability of the novel antitumor agent VNP20009, a genetically modified strain of *Salmonella typhimurium*. *J Infect Dis* 2000;**181**:1996−2002.
20. Ahmed SG, Oliva G, Shao M, Wang X, Mekalanos JJ, Brenner GJ. Intratumoral injection of schwannoma with attenuated *Salmonella typhimurium* induces antitumor immunity and controls tumor growth. *Proc Natl Acad Sci U S A* 2022;**119**:e2202719119.
21. Kim SH, Castro F, Paterson Y, Gravekamp C. High efficacy of a *Listeria*-based vaccine against metastatic breast cancer reveals a dual mode of action. *Cancer Res* 2009;**69**:5860−6.
22. Deng W, Lira V, Hudson TE, Lemmens EE, Hanson WG, Flores R, et al. Recombinant *Listeria* promotes tumor rejection by $CD8^+$ T cell-dependent remodeling of the tumor microenvironment. *Proc Natl Acad Sci U S A* 2018;**115**:8179−84.
23. Hsiao B, Khan A, Kang I. Vaccinations and biologics. *Infect Dis Clin North Am* 2020;**34**:425−50.
24. Burke CJ, Hsu TA, Volkin DB. Formulation, stability, and delivery of live attenuated vaccines for human use. *Crit Rev Ther Drug Carrier Syst* 1999;**16**:1−83.
25. Ding C, Ma J, Dong Q, Liu Q. Live bacterial vaccine vector and delivery strategies of heterologous antigen: a review. *Immunol Lett* 2018;**197**:70−7.
26. Singh S, Singh M, Gaur S. Probiotics as multifaceted oral vaccines against colon cancer: a review. *Front Immunol* 2022;**13**:1002674.
27. Pan J, Gong G, Wang Q, Shang J, He Y, Catania C, et al. A single-cell nanocoating of probiotics for enhanced amelioration of antibiotic-associated diarrhea. *Nat Commun* 2022;**13**:2117.
28. Shao H, Min F, Huang M, Wang Z, Bai T, Lin M, et al. Novel perspective on the regulation of food allergy by probiotic: the potential of its structural components. *Crit Rev Food Sci Nutr* 2024;**64**:172−86.
29. Zhang Q, Zhao Q, Li T, Lu L, Wang F, Zhang H, et al. *Lactobacillus plantarum*-derived indole-3-lactic acid ameliorates colorectal tumorigenesis via epigenetic regulation of $CD8^+$ T cell immunity. *Cell Metab* 2023;**35**:943−60.e9.
30. Bäckhed F, Ley RE, Sonnenburg JL, Peterson DA, Gordon JI. Host−bacterial mutualism in the human intestine. *Sci Technol Humanit* 2005;**307**:1915−20.
31. Gu Y, Wang C, Qin X, Zhou B, Liu X, Liu T, et al. *Saccharomyces boulardii*, a yeast probiotic, inhibits gut motility through upregulating intestinal serotonin transporter and modulating gut microbiota. *Pharmacol Res* 2022;**181**:106291.
32. Mota MJ, Lopes RP, Sousa S, Gomes AM, Delgadillo I, Saraiva JA. *Lactobacillus reuteri* growth and fermentation under high pressure towards the production of 1,3-propanediol. *Food Res Int* 2018;**113**:424−32.
33. Lin Z, Wu J, Wang J, Levesque CL, Ma X. Dietary *Lactobacillus reuteri* prevent from inflammation mediated apoptosis of liver *via* improving intestinal microbiota and bile acid metabolism. *Food Chem* 2023;**404**:134643.
34. Montgomery TL, Eckstrom K, Lile KH, Caldwell S, Heney ER, Lahue KG, et al. Lactobacillus reuteri tryptophan metabolism promotes host susceptibility to CNS autoimmunity. *Microbiome* 2022;**10**:198.
35. Watschinger C, Moschen AR. *Lactobacillus reuteri*—an old acquaintance takes on a new task in colorectal tumor surveillance. *Cancer Cell* 2022;**40**:125−7.
36. Kosek MN, Peñataro-Yori P, Paredes-Olortegui M, Lefante J, Ramal-Asayag C, Zamora-Babilonia M, et al. Safety of *Lactobacillus reuteri* DSM 17938 in healthy children 2−5 years of age. *Pediatr Infect Dis J* 2019;**38**:e178−80.
37. Bell HN, Rebernick RJ, Goyert J, Singhal R, Kuljanin M, Kerk SA, et al. Reuterin produced by a healthy microbiome inhibits colon cancer growth. *Cancer Discov* 2022;**12**:Of3.
38. Bell HN, Rebernick RJ, Goyert J, Singhal R, Kuljanin M, Kerk SA, et al. Reuterin in the healthy gut microbiome suppresses colorectal cancer growth through altering redox balance. *Cancer Cell* 2022;**40**:185−200.
39. Li N, Niu L, Liu Y, Wang Y, Su X, Xu C, et al. Taking SCFAs produced by *Lactobacillus reuteri* orally reshapes gut microbiota and elicits antitumor responses. *J Nanobiotechnol* 2024;**22**:241.
40. Bender MJ, McPherson AC, Phelps CM, Pandey SP, Laughlin CR, Shapira JH, et al. Dietary tryptophan metabolite released by intratumoral Lactobacillus reuteri facilitates immune checkpoint inhibitor treatment. *Cell* 2023;**186**:1846−62.e6.
41. Bobo D, Robinson KJ, Islam J, Thurecht KJ, Corrie SR. Nanoparticle-based medicines: a review of FDA-approved materials and clinical trials to date. *Pharm Res* 2016;**33**:2373−87.
42. Reardon S. FDA approves Alzheimer's drug lecanemab amid safety concerns. *Nature* 2023;**613**:227−8.
43. Li G, Zhao M, Xu F, Yang B, Li X, Meng X, et al. Synthesis and biological application of polylactic acid. *Molecules (Basel)* 2020;**25**:5023.
44. Zhang J, Wu C, Xu Y, Chen J, Ning N, Yang Z, et al. Highly stretchable and conductive self-healing hydrogels for temperature and strain sensing and chronic wound treatment. *ACS Appl Mater Interfaces* 2020;**12**:40990−9.
45. Prabha G, Raj V. Sodium alginate-polyvinyl alcohol-bovin serum albumin coated Fe_3O_4 nanoparticles as anticancer drug delivery vehicle: doxorubicin loading and *in vitro* release study and cytotoxicity to HepG2 and L02 cells. *Mater Sci Eng C Mater Biol Appl* 2017;**79**:410−22.
46. Chen K, Liu Y, Liu X, Guo Y, Liu J, Ding J, et al. Hyaluronic acid-modified and verteporfin-loaded polylactic acid nanogels promote scarless wound healing by accelerating wound re-epithelialization and controlling scar formation. *J Nanobiotechnol* 2023;**21**:241.
47. Wienen D, Gries T, Cooper SL, Heath DE. An overview of polyurethane biomaterials and their use in drug delivery. *J Control Release* 2023;**363**:376−88.

48. Alaraby M, Abass D, Farre M, Hernández A, Marcos R. Are bioplastics safe? Hazardous effects of polylactic acid (PLA) nanoplastics in *Drosophila*. *Sci Total Environ* 2024;**919**:170592.
49. Irshad MK, Kang MW, Aqeel M, Javed W, Noman A, Khalid N, et al. Unveiling the detrimental effects of polylactic acid microplastics on rice seedlings and soil health. *Chemosphere* 2024;**355**:141771.
50. Tian P, Zou R, Wang L, Chen Y, Qian X, Zhao J, et al. Multi-probiotics ameliorate major depressive disorder and accompanying gastrointestinal syndromes *via* serotonergic system regulation. *J Adv Res* 2023;**45**:117−25.
51. Iqbal R, Liaqat A, Jahangir Chughtai MF, Tanweer S, Tehseen S, Ahsan S, et al. Microencapsulation: a pragmatic approach towards delivery of probiotics in gut. *J Microencapsul* 2021;**38**:437−58.
52. Yang J, Kuang H, Li N, Hamdy AM, Song J. The modulation and mechanism of probiotic-derived polysaccharide capsules on the immune response in allergic diseases. *Crit Rev Food Sci Nutr* 2023;**63**:8768−80.
53. Sharpe LA, Daily AM, Horava SD, Peppas NA. Therapeutic applications of hydrogels in oral drug delivery. *Expet Opin Drug Deliv* 2014;**11**:901−15.
54. Liu H, Cai Z, Wang F, Hong L, Deng L, Zhong J, et al. Colon-targeted adhesive hydrogel microsphere for regulation of gut immunity and flora. *Adv Sci (Weinh)* 2021;**8**:e2101619.
55. Hou Y, Jin J, Duan H, Liu C, Chen L, Huang W, et al. Targeted therapeutic effects of oral inulin-modified double-layered nanoparticles containing chemotherapeutics on orthotopic colon cancer. *Biomaterials* 2022;**283**:121440.
56. Li Y, Elmén L, Segota I, Xian Y, Tinoco R, Feng Y, et al. Prebiotic-induced anti-tumor immunity attenuates tumor growth. *Cell Rep* 2020;**30**:1753−1766.e1756.
57. Amjadi S, Almasi H, Hamishehkar H, Alizadeh Khaledabad M, Lim LT. Cationic inulin as a new surface decoration hydrocolloid for improving the stability of liposomal nanocarriers. *Colloids Surf, B Biointerfaces* 2022;**213**:112401.
58. Zhang Z, Pan Y, Guo Z, Fan X, Pan Q, Gao W, et al. An olsalazine nanoneedle-embedded inulin hydrogel reshapes intestinal homeostasis in inflammatory bowel disease. *Bioact Mater* 2024;**33**:71−84.
59. Han K, Nam J, Xu J, Sun X, Huang X, Animasahun O, et al. Generation of systemic antitumour immunity *via* the *in situ* modulation of the gut microbiome by an orally administered inulin gel. *Nat Biomed Eng* 2021;**5**:1377−88.
60. Han K, Xie F, Animasahun O, Nenwani M, Kitamoto S, Kim Y, et al. Inulin-gel-based oral immunotherapy remodels the small intestinal microbiome and suppresses food allergy. *Nat Mater* 2024;**23**:1444−55.
61. Brauer E, Lippens E, Klein O, Nebrich G, Schreivogel S, Korus G, et al. Collagen Fibrils mechanically contribute to tissue contraction in an in vitro wound healing scenario. *Adv Sci (Weinh)* 2019;**6**:1801780.
62. Elzoghby AO. Gelatin-based nanoparticles as drug and gene delivery systems: reviewing three decades of research. *J Control Release* 2013;**172**:1075−91.
63. Yoon DS, Lee Y, Ryu HA, Jang Y, Lee KM, Choi Y, et al. Cell recruiting chemokine-loaded sprayable gelatin hydrogel dressings for diabetic wound healing. *Acta Biomater* 2016;**38**:59−68.
64. Zhao X, Guo B, Wu H, Liang Y, Ma PX. Injectable antibacterial conductive nanocomposite cryogels with rapid shape recovery for noncompressible hemorrhage and wound healing. *Nat Commun* 2018;**9**:2784.
65. Zheng Y, Liang Y, Zhang D, Sun X, Liang L, Li J, et al. Gelatin-based hydrogels blended with gellan as an injectable wound dressing. *ACS Omega* 2018;**3**:4766−75.
66. Al-Nimry S, Dayah AA, Hasan I, Daghmash R. Cosmetic, biomedical and pharmaceutical applications of fish gelatin/hydrolysates. *Mar Drugs* 2021;**19**:145.
67. Han K, Nam J, Xu J, Sun X, Huang X, Animasahun O, et al. Generation of systemic antitumour immunity *via* the *in situ* modulation of the gut microbiome by an orally administered inulin gel. *Nat Biomed Eng* 2021;**5**:1377−88.
68. Fayed B, Abood A, El-Sayed HS, Hashem AM, Mehanna NSH. A synbiotic multiparticulate microcapsule for enhancing inulin intestinal release and Bifidobacterium gastro-intestinal survivability. *Carbohydr Polym* 2018;**193**:137−43.
69. Liu Z, Liu F, Wang W, Sun C, Gao D, Ma J, et al. Study of the alleviation effects of a combination of *Lactobacillus rhamnosus* and inulin on mice with colitis. *Food Funct* 2020;**11**:3823−37.
70. Vedovatto S, Facchini JC, Batista RK, Paim TC, Lionzo MIZ, Wink MR. Development of chitosan, gelatin and liposome film and analysis of its biocompatibility *in vitro*. *Int J Biol Macromol* 2020;**160**:750−7.
71. Elaf R, Ben Ali A, Saad M, Hussein IA, Nimir H, Bai B. Biodegradable preformed particle gel (PPG) made of natural chitosan material for water shut-off application. *Polymers (Basel)* 2023;**15**:1961.
72. Gu S, Wang H, Wang Y, Wang X, Liu X, Wang Y, et al. Thermosensitive nanocomposite hydrogel composed of PVPylated poly(D,L-alanine) and laponite as an injectable and bioactive biomaterial. *Chem Eng J* 2023;**466**:143128.
73. Wenz JJ. Influence of steroids on hydrogen bonds in membranes assessed by near infrared spectroscopy. *Biochim Biophys Acta Biomembr* 2021;**1863**:183553.
74. Ahmadian Z, Correia A, Hasany M, Figueiredo P, Dobakhti F, Eskandari MR, et al. A hydrogen-bonded extracellular matrix-mimicking bactericidal hydrogel with radical scavenging and hemostatic function for ph-responsive wound healing acceleration. *Adv Healthcare Mater* 2021;**10**:e2001122.
75. Ninan N, Forget A, Shastri VP, Voelcker NH, Blencowe A. Antibacterial and anti-inflammatory pH-responsive tannic acid-carboxylated agarose composite hydrogels for wound healing. *ACS Appl Mater Interfaces* 2016;**8**:28511−21.
76. Bertula K, Martikainen L, Munne P, Hietala S, Klefström J, Ikkala O, et al. Strain-stiffening of agarose gels. *ACS Macro Lett* 2019;**8**:670−5.
77. Eckhart KE, Arnold AM, Starvaggi FA, Sydlik SA. Tunable, bacterio-instructive scaffolds made from functional graphenic materials. *Biomater Sci* 2021;**9**:2467−79.
78. Dima P, Stubbe PR, Mendes AC, Chronakis IS. Enhanced electric field and charge polarity modulate the microencapsulation and stability of electrosprayed probiotic cells (Streptococcus thermophilus, ST44). *Curr Res Food Sci* 2023;**7**:100620.
79. Luo Y, De Souza C, Ramachandran M, Wang S, Yi H, Ma Z, et al. Precise oral delivery systems for probiotics: a review. *J Control Release* 2022;**352**:371−84.
80. Derkach SR, Kuchina YA, Baryshnikov AV, Kolotova DS, Voron'ko NG. Tailoring cod gelatin structure and physical properties with acid and alkaline extraction. *Polymers (Basel)* 2019;**11**:1724.
81. Fawale OS, Abuibaid A, Hamed F, Kittiphattanabawon P, Maqsood S. Molecular, Structural, and rheological characterization of camel skin gelatin extracted using different pretreatment conditions. *Foods* 2021;**10**:1563.
82. Duggan A, McMillen D. Methods for electroporation and transformation confirmation in *Limosilactobacillus reuteri* DSM20016. *J Vis Exp* 2023;**23**:196.
83. Gou HZ, Zhang YL, Ren LF, Li ZJ, Zhang L. How do intestinal probiotics restore the intestinal barrier? *Front Microbiol* 2022;**13**:929346.
84. Haroun E, Kumar PA, Saba L, Kassab J, Ghimire K, Dutta D, et al. Intestinal barrier functions in hematologic and oncologic diseases. *J Transl Med* 2023;**21**:233.
85. Wei SC, Yang-Yen HF, Tsao PN, Weng MT, Tung CC, Yu LCH, et al. SHANK3 regulates intestinal barrier function through modulating ZO-1 expression through the PKCε-dependent pathway. *Inflamm Bowel Dis* 2017;**23**:1730−40.
86. Le Bastard Q, Chapelet G, Javaudin F, Lepelletier D, Batard E, Montassier E. The effects of inulin on gut microbial composition: a systematic review of evidence from human studies. *Eur J Clin Microbiol Infect Dis* 2020;**39**:403−13.

87. Qamar TR, Syed F, Nasir M, Rehman H, Zahid MN, Liu RH, et al. Novel combination of prebiotics galacto-oligosaccharides and inulin-inhibited aberrant crypt foci formation and biomarkers of colon cancer in wistar rats. *Nutrients* 2016;**8**:465.
88. Bell HN, Rebernick RJ, Goyert J, Singhal R, Kuljanin M, Kerk SA, et al. Reuterin in the healthy gut microbiome suppresses colorectal cancer growth through altering redox balance. *Cancer Cell* 2022;**40**: 185−200.e6.
89. Ursini F, Maiorino M. Lipid peroxidation an ferroptosis: the role of GSH and GPx4. *Free Radic Biol Med* 2020;**152**:175−85.
90. Liu G, Liu M, Li X, Ye X, Cao K, Liu Y, et al. Peroxide-simulating and GSH-depleting nanozyme for enhanced chemodynamic/photodynamic therapy *via* induction of multisource ROS. *ACS Appl Mater Interfaces* 2023;**15**:47955−68.
91. Zhou R, Yazdi AS, Menu P, Tschopp J. A role for mitochondria in NLRP3 inflammasome activation. *Nature* 2011;**469**:221−5.
92. Huang Y, Xu W, Zhou R. NLRP3 inflammasome activation and cell death. *Cell Mol Immunol* 2021;**18**:2114−27.
93. Fan L, Xu C, Ge Q, Lin Y, Wong CC, Qi Y, et al. *A. Muciniphila* Suppresses colorectal tumorigenesis by inducing TLR2/NLRP3-mediated M1-Like TAMs. *Cancer Immunol Res* 2021;**9**:1111−24.
94. Zhou Y, Que KT, Zhang Z, Yi ZJ, Zhao PX, You Y, et al. Iron overloaded polarizes macrophage to proinflammation phenotype through ROS/acetyl-p53 pathway. *Cancer Med* 2018;**7**:4012−22.
95. Jaganjac M, Milkovic L, Zarkovic N, Zarkovic K. Oxidative stress and regeneration. *Free Radic Biol Med* 2022;**181**:154−65.
96. Rosa CP, Belo TCA, Santos NCM, Silva EN, Gasparotto J, Corsetti PP, et al. Reactive oxygen species trigger inflammasome activation after intracellular microbial interaction. *Life Sci* 2023;**331**: 122076.
97. Yang Y, Li L, Xu C, Wang Y, Wang Z, Chen M, et al. Cross-talk between the gut microbiota and monocyte-like macrophages mediates an inflammatory response to promote colitis-associated tumourigenesis. *Gut* 2020;**70**:1495−506.
98. Gao J, Liang Y, Wang L. Shaping polarization of tumor-associated macrophages in cancer immunotherapy. *Front Immunol* 2022;**13**: 888713.
99. Chen S, Saeed A, Liu Q, Jiang Q, Xu H, Xiao GG, et al. Macrophages in immunoregulation and therapeutics. *Signal Transduct Targeted Ther* 2023;**8**:207.
100. Luo G, Wang X, Cui Y, Cao Y, Zhao Z, Zhang J. Metabolic reprogramming mediates hippocampal microglial M1 polarization in response to surgical trauma causing perioperative neurocognitive disorders. *J Neuroinflammation* 2021;**18**:267.
101. Liu J, Zhang Y, Sheng H, Liang C, Liu H, Moran Guerrero JA, et al. Hyperoside suppresses renal inflammation by regulating macrophage polarization in mice with type 2 diabetes mellitus. *Front Immunol* 2021;**12**:733808.
102. Gunassekaran GR, Poongkavithai Vadevoo SM, Baek MC, Lee B. M1 macrophage exosomes engineered to foster M1 polarization and target the IL-4 receptor inhibit tumor growth by reprogramming tumor-associated macrophages into M1-like macrophages. *Biomaterials* 2021;**278**:121137.
103. Kuo WT, Zuo L, Odenwald MA, Madha S, Singh G, Gurniak CB, et al. The tight junction protein ZO-1 is dispensable for barrier function but critical for effective mucosal repair. *Gastroenterology (New York, N Y, 1943)* 2021;**161**:1924−39.
104. Zhang S, Xu W, Wang H, Cao M, Li M, Zhao J, et al. Inhibition of CREB-mediated ZO-1 and activation of NF-κB-induced IL-6 by colonic epithelial MCT4 destroys intestinal barrier function. *Cell Prolif* 2019;**52**:e12673.
105. Gareau MG, Sherman PM, Walker WA. Probiotics and the gut microbiota in intestinal health and disease. *Nat Rev Gastroenterol Hepatol* 2010;**7**:503−14.
106. Yang W, Yang C, Du Y, Wang Q. Colon-targeted release of turmeric nonextractable polyphenols and their anticolitis potential *via* gut microbiota-dependent alleviation on intestinal barrier dysfunction in mice. *J Agric Food Chem* 2023;**71**:11627−41.
107. Xie J, Li LF, Dai TY, Qi X, Wang Y, Zheng TZ, et al. Short-chain fatty acids produced by ruminococcaceae mediate α-linolenic acid promote intestinal stem cells proliferation. *Mol Nutr Food Res* 2022; **66**:e2100408.
108. Slavica A, Trontel A, Jelovac N, Kosovec Ž, Šantek B, Novak S. Production of lactate and acetate by *Lactobacillus coryniformis* subsp. torquens DSM 20004^T in comparison with Lactobacillus amylovorus DSM 20531^T. *J Biotechnol* 2015;**202**:50−9.
109. Le Guern R, Grandjean T, Stabler S, Bauduin M, Gosset P, Kipnis É, et al. Gut colonisation with multidrug-resistant *Klebsiella pneumoniae* worsens *Pseudomonas aeruginosa* lung infection. *Nat Commun* 2023;**14**:78.
110. Chen Y, Liu Y, Wang Y, Chen X, Wang C, Chen X, et al. *Prevotellaceae* produces butyrate to alleviate PD-1/PD-L1 inhibitor-related cardiotoxicity via PPARα−CYP4X1 axis in colonic macrophages. *J Exp Clin Cancer Res* 2022;**41**:1.
111. Tawfick MM, Xie H, Zhao C, Shao P, Farag MA. Inulin fructans in diet: role in gut homeostasis, immunity, health outcomes and potential therapeutics. *Int J Biol Macromol* 2022;**208**:948−61.
112. Luo L, Luo J, Cai Y, Fu M, Li W, Shi L, et al. Inulin-type fructans change the gut microbiota and prevent the development of diabetic nephropathy. *Pharmacol Res* 2022;**183**:106367.
113. Duan C, Huang L, Zhang C, Zhang L, Xia X, Zhong Z, et al. Gut commensal-derived butyrate reverses obesity-induced social deficits and anxiety-like behaviors *via* regulation of microglial homeostasis. *Eur J Pharmacol* 2021;**908**:174338.
114. Song Q, Zhang X, Liu W, Wei H, Liang W, Zhou Y, et al. *Bifidobacterium pseudolongum*-generated acetate suppresses non-alcoholic fatty liver disease-associated hepatocellular carcinoma. *J Hepatol* 2023;**79**:1352−65.
115. Vodenkova S, Buchler T, Cervena K, Veskrnova V, Vodicka P, Vymetalkova V. 5-fluorouracil and other fluoropyrimidines in colorectal cancer: past, present and future. *Pharmacol Ther* 2020;**206**: 107447.
116. Hong BY, Sobue T, Choquette L, Dupuy AK, Thompson A, Burleson JA, et al. Chemotherapy-induced oral mucositis is associated with detrimental bacterial dysbiosis. *Microbiome* 2019;**7**:66.
117. Gigola G, Carriere P, Novoa Díaz MB, Perdigon G, Zwenger AO, Gentili C. Survival effect of probiotics in a rat model of colorectal cancer treated with capecitabine. *World J Gastrointest Oncol* 2021;**13**:1518−31.
118. Osterlund P, Ruotsalainen T, Korpela R, Saxelin M, Ollus A, Valta P, et al. *Lactobacillus* supplementation for diarrhoea related to chemotherapy of colorectal cancer: a randomised study. *Br J Cancer* 2007;**97**:1028−34.
119. An J, Ha EM. Lactobacillus-derived metabolites enhance the antitumor activity of 5-FU and inhibit metastatic behavior in 5-FU-resistant colorectal cancer cells by regulating claudin-1 expression. *J Microbiol* 2020;**58**:967−77.
120. Kuipers EJ, Grady WM, Lieberman D, Seufferlein T, Sung JJ, Boelens PG, et al. Colorectal cancer. *Nat Rev Dis Primers* 2015;**1**:15065.
121. Jaferian S, Negahdari B, Eatemadi A. Colon cancer targeting using conjugates biomaterial 5-flurouracil. *Biomed Pharmacother* 2016;**84**: 780−8.
122. Tsujii K, Hattori T, Imaoka A, Akiyoshi T, Ohtani H. 5-Fluorouracil-induced gastrointestinal damage impairs the absorption and anticoagulant effects of dabigatran etexilate. *J Pharmaceut Sci* 2018;**107**:1430−3.
123. Pizzo SV, Parisa A, Roya G, Mahdi R, Shabnam R, Maryam E, et al. Anti-cancer effects of *Bifidobacterium* species in colon cancer cells and a mouse model of carcinogenesis. *PLoS One* 2020;**15**:e0232930.
124. Singh S, Singh M, Gaur S. Probiotics as multifaceted oral vaccines against colon cancer: a review. *Front Immunol* 2022;**13**:1002674.
125. Sun Q, Yin S, He Y, Cao Y, Jiang C. Biomaterials and encapsulation techniques for probiotics: current status and future prospects in biomedical applications. *Nanomaterials (Basel)* 2023;**13**:2185.
126. He Y, Li Z, Xu T, Luo D, Chi Q, Zhang Y, et al. Polystyrene nanoplastics deteriorate LPS-modulated duodenal permeability and inflammation in mice *via* ROS drived-NF-κB/NLRP3 pathway. *Chemosphere* 2022;**307**:135662.

127. Chen J, Zhou Z, Wu N, Li J, Xi N, Xu M, et al. Chlorogenic acid attenuates deoxynivalenol-induced apoptosis and pyroptosis in human keratinocytes *via* activating Nrf2/HO-1 and inhibiting MAPK/NF-κB/NLRP3 pathways. *Biomed Pharmacother* 2024;**170**: 116003.
128. Fu Y, Cao J, Wei X, Ge Y, Su Z, Yu D. Klotho alleviates contrast-induced acute kidney injury by suppressing oxidative stress, inflammation, and NF-kappaB/NLRP3-mediated pyroptosis. *Int Immunopharmacol* 2023;**118**:110105.
129. Song H, Zhao C, Yu Z, Li Q, Yan R, Qin Y, et al. UAF1 deubiquitinase complexes facilitate NLRP3 inflammasome activation by promoting NLRP3 expression. *Nat Commun* 2020;**11**:6042.
130. Qu Z, Zhou J, Zhou Y, Xie Y, Jiang Y, Wu J, et al. Mycobacterial EST12 activates a RACK1−NLRP3−gasdermin D pyroptosis−IL-1β immune pathway. *Sci Adv* 2020;**6**:eaba4733.
131. Zhang D, Jian YP, Zhang YN, Li Y, Gu LT, Sun HH, et al. Short-chain fatty acids in diseases. *Cell Commun Signal* 2023;**21**: 212.
132. Tan J, McKenzie C, Potamitis M, Thorburn AN, Mackay CR, Macia L. The role of short-chain fatty acids in health and disease. *Adv Immunol* 2014;**121**:91−119.
133. Coutzac C, Jouniaux J-M, Paci A, Schmidt J, Mallardo D, Seck A, et al. Systemic short chain fatty acids limit antitumor effect of CTLA-4 blockade in hosts with cancer. *Nat Commun* 2020;**11**: 2168.
134. Sivaprakasam S, Bhutia YD, Yang S, Ganapathy V. Short-chain fatty acid transporters: role in colonic homeostasis. *Compr Physiol* 2017; **8**:299−314.
135. Martin-Gallausiaux C, Marinelli L, Blottière HM, Larraufie P, Lapaque N. SCFA: mechanisms and functional importance in the gut. *Proc Nutr Soc* 2021;**80**:37−49.
136. Mindt S, Aida S, Merx K, Müller A, Gutting T, Hedtke M, et al. Therapeutic drug monitoring (TDM) of 5-fluorouracil (5-FU): new preanalytic aspects. *Clin Chem Lab Med* 2019;**57**:1012−6.
137. Sakai H, Sagara A, Matsumoto K, Jo A, Hirosaki A, Takase K, et al. Neutrophil recruitment is critical for 5-fluorouracil-induced diarrhea and the decrease in aquaporins in the colon. *Pharmacol Res* 2014;**87**: 71−9.
138. Batista VL, De Jesus LCL, Tavares LM, Barroso FLA, Fernandes L, Freitas ADS, et al. Paraprobiotics and postbiotics of *Lactobacillus delbrueckii* CIDCA 133 mitigate 5-FU-induced intestinal inflammation. *Microorganisms* 2022;**10**:1418.